
Low-cost techniques for assessing the quality of drinking water from biosand filters

Cort B. Hammond – hammondc15@mail.wlu.edu

Washington and Lee University
Chemistry-Engineering Honors Thesis

5/17/2015

Advisor: Jon Erickson, Ph.D. – ericksonj@wlu.edu

Contents

| | | |
|-----|---|----|
| 1 | Abstract..... | 3 |
| 2 | Introduction..... | 3 |
| 2.1 | Water Quality..... | 3 |
| 2.2 | Biosand filter design and function..... | 5 |
| 2.3 | Biosand filter modifications..... | 7 |
| 2.4 | Monitoring the maturity and activity of the biofilm..... | 8 |
| 2.5 | Assessing biosand filter effectiveness..... | 9 |
| 2.6 | Microfiltration theory..... | 11 |
| 3 | Methods..... | 14 |
| 3.1 | Preparation and Running of Biosand Filter Columns..... | 14 |
| 3.2 | IR of filter retentate..... | 16 |
| 3.3 | Preliminary filter clogging experiment..... | 16 |
| 3.4 | Correlation of filter clogging with bacterial counts and turbidity..... | 18 |
| 3.5 | Filter membrane regeneration..... | 19 |
| 4 | Results..... | 19 |
| 4.1 | Baseline filter properties..... | 19 |
| 4.2 | IR Spectroscopy of filter retentate..... | 21 |
| 4.3 | Micropore filter flow rate assay..... | 22 |
| 4.4 | Micropore filters clogged by bacteria or turbidity..... | 25 |
| 4.5 | Bacterial cultures..... | 28 |
| 4.6 | Model for coliforms and pathogenic risk..... | 28 |
| 4.7 | Micropore filter regeneration..... | 30 |
| 5 | Discussion..... | 31 |
| 5.1 | IR spectroscopy of micropore filter retentate..... | 31 |
| 5.2 | Proof of concept for the filter clogging assay..... | 31 |
| 5.3 | Micropore filter fouling mechanism in relation to assay..... | 32 |
| 5.4 | Accuracy of the micropore filter clogging assay..... | 33 |
| 5.5 | Limitations of the filter clogging assay..... | 35 |
| 5.6 | Ruggedness & Feasibility of the filter clogging assay..... | 36 |
| 5.7 | Cost and efficiency of the filter clogging assay (FCA)..... | 37 |
| 5.8 | The prototype assay kit and protocol..... | 37 |
| 6 | Conclusions..... | 39 |
| 7 | Acknowledgments..... | 40 |

| | | |
|-----|---|----|
| 8 | References..... | 40 |
| 9 | Appendices..... | 43 |
| 9.1 | Calibration data | 43 |
| 9.2 | FT-IR of filters | 44 |
| 9.3 | SEM-EDS micrographs..... | 45 |
| 9.4 | Scanned images of Coliscan bacterial cultures | 47 |
| 9.5 | Cost comparison..... | 54 |

1 Abstract

Over 4 million people worldwide are estimated to benefit from the biosand filter (BSF), an inexpensive point-of-use (POU) water treatment technology designed to remove turbidity, bacterial contamination, and parasites. The effectiveness of biosand filters can depend on initial quality of the source water. Also, the commissioning, operation, and maintenance of the filters, if performed incorrectly, can result in low-quality water. Water quality is typically assessed via field measurements of turbidity and conductivity and laboratory methods such as bacterial assays, microcopy, and colorimetry. Turbidity and conductivity instruments enjoy widespread use since they are low cost, low complexity, and provide results quickly. However, lab analyses are required in order to get a true measure of how safe the water is for human consumption especially if the contaminants of concern are bacteria or trace metals. Lab analyses are often not available or prohibitively costly in areas where biosand filters are used. The limited meaning of field assays and the high cost of lab analyses leave a gap for an intermediate cost tools that can provide more meaningful results in the field. This work describes a Filter Clogging Assay (FCA) where the fouling rate of a 0.2 micron syringe filter is measured as a proxy for bacterial contamination. Ultimately, the (FCA) proved to be promising, with a strong correlation ($R^2 = 0.93$, $p = 6.5E-10$) between the filter clogging rate and total coliforms and an average analysis time of 14.5 ± 1.5 minutes. The average cost of each analysis is approximately \$1.50. This novel method would allow a sample to be assigned one of the four World Health Organization pathogenic risk categories allowing more rapid decision making.

2 Introduction

2.1 Water Quality

A broad range of humanitarian organizations have steadily increased the proportion of the world's population with access to improved water sources—still around 783 million people do not have access to improved drinking water (WHO, 2014). Improved drinking water is a term used to describe water produced by a range of treatment technologies designed to significantly reduce the potential of contracting a water-borne illness. While chemical disinfection and membrane filtration are commonplace in developed nations and increasing in use world-wide, appropriate technologies such as biosand filtration, which eliminate or reduce pathogens and removes parasites, are vital to reducing disease outbreaks and infant mortality (Tiwari et al., 2009). The World Health Organization (WHO) has developed categories relating to bacterial quality of water (WHO, 2011); Figure 1 presents the chart used in classifying the pathogenic risk of a water supply based on the concentration of the pathogenic indicator, *E. coli*, and a qualitative assessment of the potential for the supply to contain enteric pathogens. This two-parameter ranking system is necessary since *E. coli* are merely indicators of pathogens and often concentrations can be decoupled from actual pathogen levels resulting in underestimates of the risk of drinking the water and need for corrective action to prevent illness (Lloyd and Bartram, 1991).

| | | Sanitary inspection risk score (susceptibility of supply to contamination from human and animal faeces) | | | |
|------------------------------------|--------|--|--------|------|-----------|
| | | 0-2 | 3-5 | 6-8 | 9-10 |
| E. coli bacteria (number/100mL) | < 1 | Low | Medium | High | Very high |
| | 1-10 | | | | |
| | 11-100 | | | | |
| | > 100 | | | | |

Figure 1: Pathogenic risk score chart taking into account both the concentration of *E. coli* indicator bacterium and the potential source of pathogens. Developed by the World Health Organization (WHO) and based on Lloyd and Bartram, 1991.

Monitoring water quality both at the source and the tap is necessary to verify that the treatment is necessary, effective, and/or appropriate. In some cases, visual inspection and knowledge of the hydrology at the source may suffice to confirm or refute the safety of a source. However, in most cases water requires treatment and in these cases it is standard practice to test effluent water from the process regularly to verify the effectiveness of the treatment. The ability of an organization or individual to monitor drinking water quality is contingent on the availability of time, expertise, and resources. Five criteria should be used to assess how appropriate a monitoring technology is for deployment in the field in developing nations. It is most important that the method be meaningful (1); excellent examples of meaningful tests are a bacterial culture or pathogen assay. Low cost (2) and speed (3) are critical, as demonstrated recently in an Engineers Without Borders project in Guatemala (), the cost of performing bacterial analyses is often prohibitive and even when they are performed, the turnaround can be weeks to months. Finally, the method must be straightforward (4) and the equipment must be rugged (5); a perfect example of such a technology is the turbidity tube which is easy to use and nearly indestructible.

Turbidity is perhaps the most commonly used measure of water quality. The WHO argues that it is an important indicator of untreated water quality, since pathogen levels are generally proportional to turbidity. Numerous studies (such as Brookes et al., 2005, Pronk et al., 2005, Schwartz et al., 1997) support a weak to moderate correlation between turbidity and pathogen levels in surface water. Turbidity is also useful in determining the suitability of source water for further treatment. For example, the WHO recommends that water to be chlorinated be less than 5 NTUs and ideally 1 NTU (WHO, 2011). Two main technologies are used to measure turbidity, the nephelometric turbidimeter and the turbidity tube. The turbidimeter, though more costly and more difficult to maintain, can distinguish turbidity in samples below 5 NTUs. The turbidity tube is inexpensive and rugged; however, it has a detection limit of around 5 NTUs for a 90 cm tube (Myre and Shaw, 2006). In theory, longer tubes can be built to measure lower turbidities; to measure the turbidity of water at 3 NTUs, a 123 cm long tube would be required based on the relation described by Myre and Shaw (2006). Clearly, there are limitations to this method; treatment of water can change the turbidity through sedimentation or leave it relatively unchanged while altering pathogen concentrations in different ways. The turbidity of water produced by filtration systems can depend on both the effective pore size and the types of the suspended solids in the influent—small silicates and clays can pass through pores. Bacteria that are adhered to larger particles are more likely to be trapped, while free-floating individuals are more likely to pass

through. Based on these logical arguments fact, I postulate that water treatment weakens the correlation between pathogen levels and turbidity. For this reason, turbidity alone should not be trusted to determine how clean/safe filtered water is.

The standard for assessing the pathogenic risk of drinking water is to determine the most probable number of *E. coli* per volume of water. *E. coli* has been shown to be the best indicator of pathogenic risk since the only source is animal feces (Edberg et al., 2000). While effective, the bacterial assays currently available (such as Coliscan, Colilert, and Petrifilm) often require more resources and expertise than can be spared in developing nations. Sterile labs with temperature and humidity controlled incubators are typically few in number and sample turnaround can be slow reducing the likelihood of detecting a problem soon enough to prevent illness.

Dissolved inorganic contaminants, such as arsenic or fluoride, can be much more difficult to detect when present at in trace amounts, requiring methods such as spectrophotometry, spectroscopy, and ion selective probes (Vrana et al., 2005). However, at higher concentrations, inexpensive colorimetric test strips and electrodes can be employed to measure the abundance of a contaminant. Conductivity is commonly measured, but is not a useful indicator of the safety of the water since hardness is often the principal contributor to conductivity.

Despite the existence of numerous water quality tests for a variety of parameters, more need to be developed to bring faster and cheaper water quality analyses into the field where they can help to prioritize maintenance efforts and give water consumers some peace of mind knowing that their system is effective.

2.2 Biosand filter design and function

Slow sand filters were one of the earliest treatment technologies, implemented at the municipal level by the Chelsea Water Company to treat the water of the Thames, they were the dominant treatment technology until rapid sand filtration and chemical disinfection became more common. These gravity-driven filters function by removing contaminants via three overall categories of processes: purification, transport, and attachment. The top layer in the sand filter, termed the *schmutzdecke*, is rich in nutrients and biological activity.

Purification occurs primarily in the biolayer where microorganisms metabolize organic compounds, nutrients, and pathogens and produce water, ions (PO_4^{3-} , NO_3^- , and SO_4^{2-}), and gases (CO_2 , N_2), which off-gas when the water is released.

- Assimilation into cell structures
- Algae remove CO_2 , nitrates, sulfates, and phosphates
- Algae incorporate organics and transform them into degradable forms
- Algae produce bacterial toxins

Transport involves the physical removal of particles by screening, sedimentation, inertial/centrifugal forces depositing material in pore spaces, and electrostatic attraction between positive proteins and the negatively charged sand (Huisman and Wood, 1974).

Attachment is a more permanent process involving electrostatic attraction, Van der Waals forces, and adhesion to sticky bacterial and algal molecules (Huisman and Wood, 1974).

Similar to slow sand filters, biosand filters (BSFs) (Figure 2) are a low-maintenance, household-scale, point-of-use technology invented by Canadian engineer Davis Manz. This appropriate technology is estimated to benefit over 4 million people (CAWST). A BSF consists of a sand column which acts as a micropore filter and a support for the active biolayer. Composed of organic and inorganic particulates trapped in a matrix of bacteria, algae, protists, diatoms, and zooplankton, the biolayer has been shown to develop to maturity over the course of 6-8 weeks (Joubert and Pillay, 2007). The sand column is between 22-25 inches (56-64 cm) tall. An underlying gradation of fine to coarse gravel ensures that the outflow pipe is not clogged. The filter can be operated intermittently; however, the biolayer requires regular influx of nutrients and oxygen at least every three days (Young-Rojanschi and Madramootoo, 2015). When properly operated, BSFs have been shown to eliminate up to 99% of *E.coli* and other pathogens such as *Giardia* (Palmateer et. al., 1999). However, before the biolayer has developed, *E. coli* removal rates have been documented as low as 63% (Stauber et al., 2006). Additionally, some filters may be specifically designed to precipitate or adsorb contaminants using additional media such as zerovalent iron as discussed in greater depth in the next section.

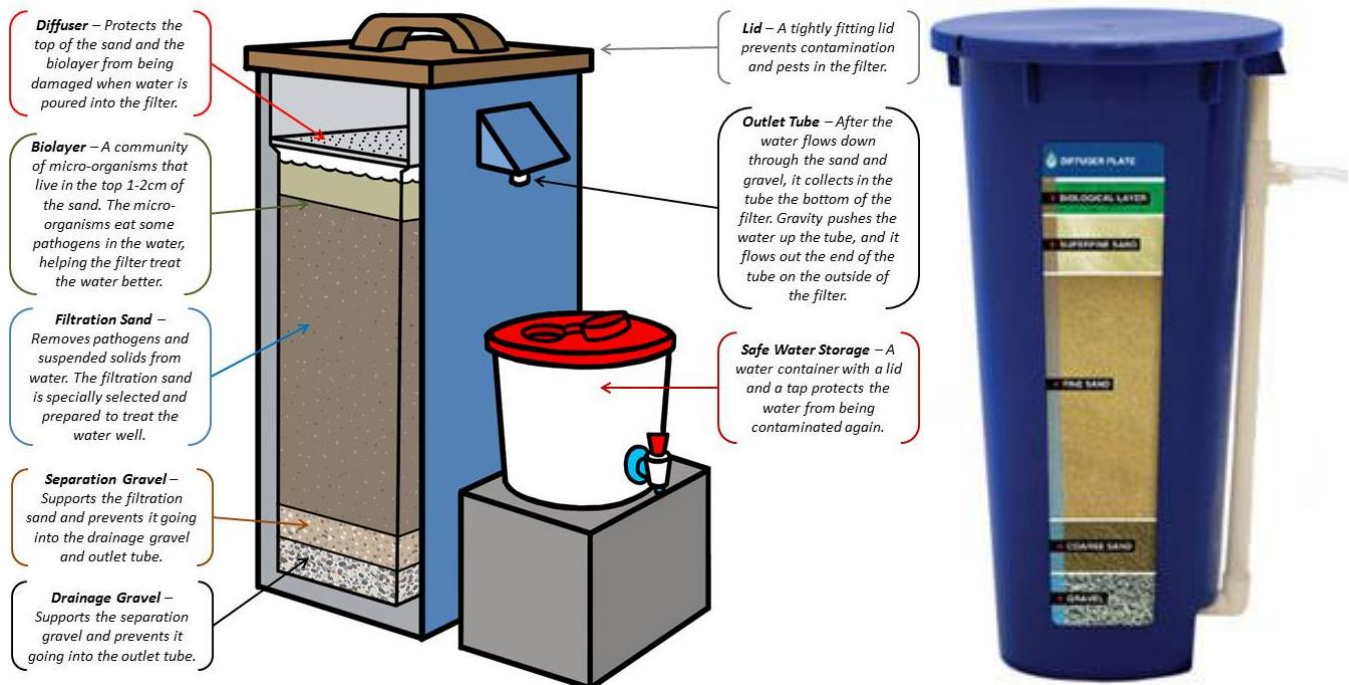


Figure 2: (left) the general design of a concrete biosand filter (CAWST.org) along with a plastic biosand filter product (Hydraid.org) (right).

One of the primary mechanisms for contaminant removal is the biolayer at the top of the sand column. The growth of this layer is encouraged by the buildup of nutrients and natural microbial agents. Since the biolayer is the most dynamic component of the filter, there have been numerous efforts to better understand it. Recent research has shown that after 60 days of operation, the dissolved oxygen concentration decreases from around 4.5 mg/L at 1cm above the sand-water interface to around 1 mg/L 5 cm below the sand-water interface due to microbial respiration (Young-Rojanschi and Madramootoo, 2013).

Continuously operated biosand filters compared with those operated only every 24 hours are more effective at removing *E. coli*, viruses, and turbidity. In a laboratory study, continuously operated filters reduced *E. coli* amounts by approximately 1000 times, while the intermittently operated filter reduced *E. coli* amounts by around 100 times. Intermittent operation still produces water with significantly fewer *E. coli* (Young-Rojanschi and Madramootoo, 2013).

The effectiveness of biosand filters has also been demonstrated by several epidemiological studies. One study in the Dominican Republic found the incidence of diarrheal disease was 2.6 times higher in those who did not drink biosand filter water (Aiken et al., 2011). In a study in Cambodia diarrheal disease was 1.4-4.2 times higher amongst those who did not use biosand filters (Stauber et al., 2011). Divelbiss et al. (2012) studied multiple factors contributing to the effectiveness biosand filters in Guatemala and found that BSFs decreased the incidence of diarrheal disease, though 69% of households used additional water treatment because they were uncertain about the quality of the water produced. Overall, the effectiveness of the biosand filter in improving water quality has been demonstrated, though it appears that it would be best received and most effective if combined with a secondary disinfection step, perhaps with a UV lamp.

2.3 Biosand filter modifications

Despite their low-cost and effectiveness, BSFs are not a mythical panacea—viruses (Bradley et al., 2011) and dissolved inorganic ions such as arsenic (Noubactep et al., 2012), fluoride (Miller, 2007) and hydrophilic organic molecules (Nakada et al., 2007) are not efficiently removed by the biolayer and sand alone. As a result, attempts have been made to develop additional treatment stages to better handle specific contaminants. Of particular concern in the developing world are arsenic (Berg et al., 2001), and fluoride which enter ground water through natural geologic deposits. Pesticides and viruses can also present a significant threat to the safety of surface water. In fact, arsenic was recently detected by a team that I led to Guatemala in 2014 to build two biosand filters at 3-5 times the United States Environmental Protection Agency's limit of 10 ppb.

Viruses are difficult to remove due to their small size (0.02 to 0.4 μm) and their net negative charge which repels the net negative charge on clean sand particles (Zerda et al., 1984). A zerovalent iron amendment buried in the sand bed has been investigated as a means to improve virus removal (Bradley et al., 2011). Viruses are bound to the net-positive surface of the iron and as rust particles spall off, they are trapped in the sand.

Iron is also commonly used in precipitation reactions in water treatment. Ferric chloride is commonly used as a precipitant to treat arsenic; upon addition to water, hydrochloric acid is formed along with Iron(III) Hydroxide which in turn complexes with As(V) to form a precipitate (O'Day et al., 2004). The Kanchan Arsenic Filter (KAF), developed at MIT, is a BSF-based arsenic precipitation filter that uses an overlying vessel filled with a diffusive brick layer and iron nails in place of the diffuser plate to complex arsenic prior to the standard BSF stage which removes the iron flocs (Ngai et al., 2006).

Bone char has been researched and implemented as a means of removing fluoride from groundwater and may be effectively combined with biosand filtration to provide bacterial removal as well (Miller, 2007).

Any of these modifications should be noted when assessing the quality of water from a biosand filter since they may impact the assay, or may warrant further chemical analyses before the water can be

declared safe. While a full spectrum of tests should be performed when possible, my work focused on assessing microbiological contamination only.

2.4 Monitoring the maturity and activity of the biofilm

Since the development of the biofilm is critical to the effectiveness of the biosand filter, some effort has been made to characterize its development. In 2014, when I was part of a EWB team constructing two biosand filters near Santiago Atitlán, Guatemala, a common question posed was how long the biolayer takes to mature. Developing a method to quantify biolayer thickness and activity was initially explored as an option for rapidly determining whether a biosand filter is effective. Details for a selection of these methods are provided below (Table 1) and tradeoffs are considered to determine the best prospective method.

Table 1: An overview of researched and proposed methods for studying the maturation of a biofilm.

| Method | Advantages | Disadvantages | References |
|---|---|--|---|
| Respirometry/ CO_2 | Amount of CO_2 evolved is proportional to metabolic rate | Difficult to measure, dependent on influent quality and environmental conditions | (Kroukamp and Wolfaardt, 2008) (Urfer and Huck, 2000) |
| Reactive tracer | Tracer can be to certain bacterial enzymes, selective and quantitative | A chemical assay or electrode is required to measure metabolites | (Fonseca et al., 2001) |
| Microscopy (light or scanning electron) | Requires only a few sand grains, some species are indicators of biofilm maturity | Not quantitative, requires specialist knowledge and expensive equipment | (Joubert and Pillay, 2008) |
| Capacitance | Simple to measure + process, easy to modify filters with electrode ports | Indirect measurement, measurements in the pF range, variability in the conductivity of input solution | (Kim et al., 2011) Yang et al. (2004) Sanz et al. (2012) |
| Infrared spectroscopy | Direct measurement of organic biomarkers such as amides and carbonyls, possible to subtract out water as background | Major filter column modification Doesn't average properties of entire cross-section, interference with strong absorption of IR by water | (Schmitt and Flemming, 1996) (Howe et al., 2002) (Davis et al., 2010) |

Biofilms are composed of millions of cells which, over time, can occupy electrodes surfaces. These cells can be modeled as a resistor capacitor circuit with the phospholipid bilayer separating charge (Figure 3) (Radke and Alocilja, 2005); it follows that measuring capacitance can be a proxy for estimating the density of a biofilm without disturbing it. Theoretically, the capacitance will not change as a function of water conductivity or the presence of other solids such as silts and clays and the electrode could be installed on the interior of the BSF. This method would be more costly and more complicated than the bacterial assays commonly used. Yang et al. (2004) report a detection limit of 10^8 CFU/100mL and Radke and Alocilja (2005) report a detection limit of 10^6 CFU/100mL using carefully manufactured high-density interdigitated array microelectrodes and high-end impedance analyzers.

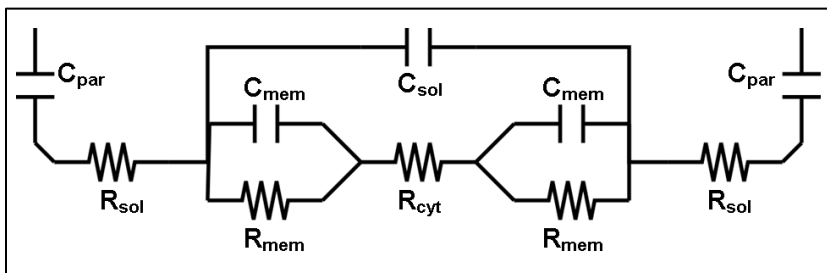


Figure 3: Equivalent circuit describing the electronic behavior of a cell situated between the two electrodes adapted from Radke and Alocilja, 2005. The parasitic capacitance, in combination with the double layer capacitance, (C_{par}) can be a major source of interference.

Attenuated total reflectance (ATR) Infrared (IR) spectroscopy has been used to detect the formation of biofilms and analyze the composition of surface waters (Howe et al., 2002). Furthermore, it has been investigated as method for quantifying *E. coli* contamination of meat (Davis et al., 2010). ATR-IR spectroscopy allows the analysis of surfaces. Incident IR radiation is internally reflected in a diamond crystal and the evanescent wave that penetrates the interface of the sample and the diamond is adsorbed by the molecules present. The spectrum contains adsorption peaks located at wavelengths corresponding to the vibrational energy of bonds that are characteristic of certain functional groups. Biotic materials are expected to exhibit carbonyl, amide, and hydroxyl bands and a method involving clamping a filter retentate-side down on an ATR crystal (Figure 4) has been shown capable of detecting some of these signals (Howe et al., 2002). The main concern is that it would be difficult to construct a single band instrument that is both inexpensive and accurate; even with the most basic IR source, diffraction grating, IR photodiode, noise filter, and signal amplifier the cost may be in excess of \$100 and may not be very rugged.

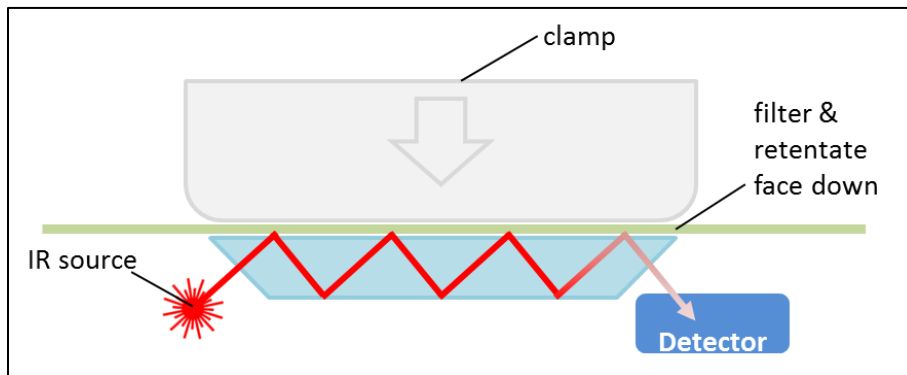


Figure 4: Diagram of the ATR-FT-IR method used to measure the spectra of the retentate on both nitrocellulose and nylon filters.

2.5 Assessing biosand filter effectiveness

The focus of this research is the development of a method for quantifying bacterial concentrations in filter effluents indirectly. After reviewing current literature and testing several methods, it became apparent that a new approach was needed.

Monitoring effluent quality is irrespective to influent quality is the ultimate evaluation the effectiveness of a biosand filter in the field. In developing nations, where biosand filters are sometimes the sole water treatment method used, monitoring is often hampered by lack of trained lab personnel, controlled environments, and equipment.

Microbial assays such as Coliscan and Colilert provide quantitative to semi-quantitative evaluations of the number of enteric pathogen indicator bacteria. These methods are commonly used worldwide to verify the effectiveness of conventional municipal treatment plants. Most efforts to characterize the effectiveness and mechanisms of purification of biosand filters have typically focused on lab-based techniques such as bacterial cultures. Often these biosand filters are run in the lab and are dosed with concentrations of *E. coli* solutions at around 10^4 CFUs/100mL (Elliot et al., 2008) to 10^5 CFUs/100mL

Stauber et al., 2006), which are 3 to 4 orders of magnitude greater than what would be expected in surface waters—this can lead to artificially high removal rates. The absolute number of *E. coli* in the effluent needs to be determined to evaluate effectiveness.

Turbidity is frequently used as an indication of the suitability of a water source for drinking water. Higher turbidity is generally positively correlated with bacterial contamination, but there is a high level of variability due to the many different turbidity-causing agents. While untreated water can have high levels of turbidity due to clays, silicates, and algae, water that has passed through a biosand filter typically has very low levels of turbidity (<5 NTUs) and the primary contaminants of concern are dissolved solids, bacteria, and viruses. Since turbidity levels below 10 NTUs are not apparent to the naked eye and turbidity levels below 1 NTU are below signal detection limits for most field turbidimeters, it is not possible to assess the levels of contaminants in effluent samples by their turbidity alone. Furthermore, since bacteria are small enough to be effectively transparent to visible light, even high numbers of cells (up to 10^7 per mL) negligibly scatter light compared to other, larger sources of turbidity (Métris et al., 2003). As a result, there is less correlation between turbidity and bacterial numbers for filtered water. For this reason, it may be possible to accurately estimate the degree of contamination of the water based on a standard curve correlating the reduction in flow rate of sample after a fixed hydraulic loading to range of *E.coli* counts.

The use of membrane filters in the IR experiments led to the concept of a method based on the fact that solids will cause a decline in flux when a constant pressure is applied. Such a method is commonly applied in the reverse osmosis (RO) industry. The Silt Density Index (SDI) test is used to determine how suitable low turbidity (< 1 NTUs) feed water is for filtration or whether it needs to be polished to remove turbidity. The ASTM standard for determining the SDI instructs the user to filter 500mL of sample through a 0.45 μ m membrane at a pressure of 207 kPa (30 psi) (ASTM D 4189). The standard also points out that the SDI is dependent on the material and construction of the filter as well as the temperature. Research into the relation between the SDI and actual foulant deposition has shown a geometric relation, with every 1 unit of increase in the SDI resulting in a doubling of material deposition (Kremen and Tanner, 1998).

While a 0.45 μ m filter will retain most particles, not all bacteria will be retained on the filter and fouling will progress at a slower rate, requiring a larger sample size. Since the goal is to develop a proxy for bacterial contamination, a 0.2 μ m filter was the first choice since the smallest bacterium, *Brevundimonas diminuta*, measures approximately 0.3 μ m in diameter. Since most pathogenic bacteria such as *E. coli*, *Legionella pneumophila*, and *Pseudomonas aeruginosa* are at least 0.5 μ m in diameter, all should be retained on a 0.2 μ m filter. Furthermore, it is estimated that the sample size required to make an accurate measurement of clogging rate will be at least half of the 500mL required by the ATSM standard due to the smaller pore size. Theoretical outcomes of this proposed filter clogging test for bacteria (Table 2) include 2 true positive scenarios, 2 false positive scenarios, and a single false negative scenario. There are only two scenarios in which the water would be declared safe. The possibility of the false negative due to the good correlation between indicator bacteria and pathogens is very limited. These qualities are promising.

Table 2: Hypothesized scenarios for the filter clogging assay used to theorize how meaningful the method could be.

| | | | | | | |
|--|--|--|--|---|---|--|
| Scenario | 1: high quantities of inorganic suspended solids, few bacteria | 2: similar quantities of inorganic suspended solids and bacteria | 3: large quantities of indicator bacteria relative to inorganics | 4: large number of indicator bacteria; no pathogens | 5: low amounts of bacteria and inorganic solids | 6: low amounts of indicator bacteria relative to pathogens |
| Result of assay | rapid clogging, visible turbidity | rapid clogging, no visible turbidity | rapid clogging, no visible turbidity | rapid clogging | slow clogging | slow clogging |
| Diagnosis of pathogenic water quality | Unsafe water; false positive | Moderately unsafe water | Unsafe water | Unsafe water; false positive | Safe water | Safe water; false negative |
| Probability of outcome | low | moderate | high | moderate | moderate | low |
| Method for evaluation | SEM/EDS, turbidity, Coliscan | SEM/EDS, turbidity, Coliscan | SEM/EDS, turbidity, Coliscan | Coliscan, Pathogen assay | Mass difference | Coliscan, Pathogen assay (including viruses) |

In section 2.1 five criteria were proposed (meaningful, low cost, quick, simple, and rugged) for assessing whether an appropriate technology for determining water quality in the field in developing nations. If these five common and proposed methods are scored from 1 to 10 based on these criteria we can see that the commonly used turbidity and newly proposed filter fouling methods come out on top with bacterial cultures a close second (Figure 5).

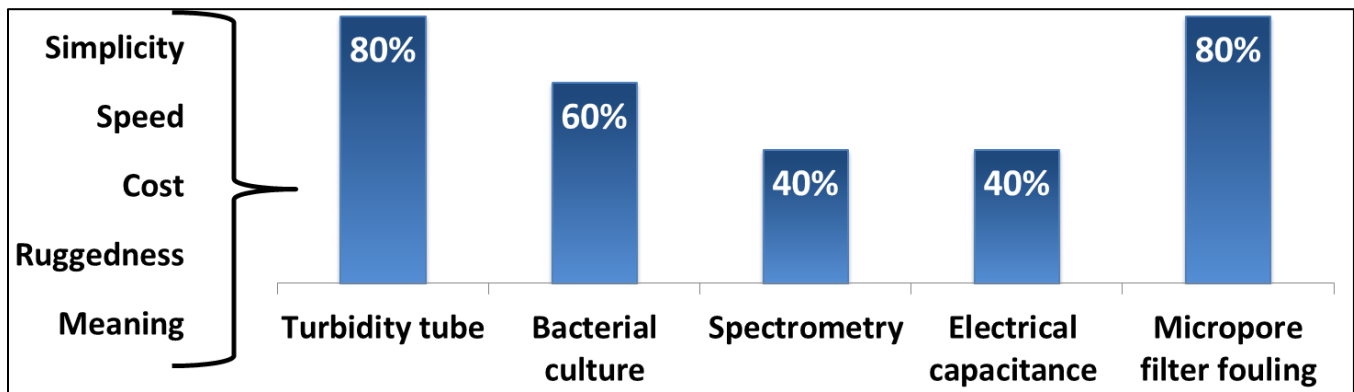


Figure 5: Ranking of water quality assessment tools using the five criteria indicated.

2.6 Microfiltration theory

Microfiltration was discussed as one mechanism by which the BSF removes contaminants from water some are trapped on the surface of the sand and some, deep in the tortuous pores. To evaluate water produced by a biosand filter the concept of a micropore filter clogging assay as a proxy for bacterial numbers in filter effluent was proposed in the previous section. This assay would involve measuring the rate at which a disposable 0.2 micron membrane filter clogs when a sample of water from the BSF is filtered at a constant pressure. A better understanding of filtration and fouling mechanisms aided in selecting the type of filter and the pressure to be applied, as well as in interpreting the results of the assay.

For in-line flow filters, there are two broad approaches to removing particles from the water: depth filtration and screen filtration. Depth filters make use of tortuous pore channels through the sand to trap materials within the filter, whereas screen filters trap all particle on the surface of the membrane, leading to faster clogging (Baker, 2004). When particles are trapped in the pores they contribute to irreversible fouling (Konieczny, 2002).

Filters are typically characterized by their average pore size and their permeability. The flux of pure water through the filter can be described by Darcy's law:

$$J = \frac{\Delta P}{\mu R}; \text{ where } R \text{ is the resistance of the media in } m^{-1}$$

The flux, volumetric flow rate normalized to the area of the filter perpendicular to the flow direction, is the commonly used statement of flow rate since it allows comparison between filters of various sizes. In much the same way that electrical current is determined by dividing the potential by the resistance, the flux is determined by dividing the pressure by the resistance.

Following the same analogy, when particles are suspended in the solution, the flux becomes a function of time, or the total volume filtered. This introduces two new resistance factors: R_p and R_c . R_p is the pore-clogging resistance characteristic of depth filtration. R_c is the resistance due to cake-formation, which is characteristic of screen filtration (Lim and Bai, 2003). These resistances typically act in series.

There are four major types of membrane micropore filters that are differentiated by manufacturing technique and function: track-etched (polycarbonate), Loeb-Sourirajan (polysulfone), expanded film (polyethylene), and phase separation (nitrocellulose and other polymers). Track-etched and Loeb-Sourirajan type filters remove particles via screen filtration. Expanded film and phase separation membranes act as both screen and depth filters. The filter membranes used in this method are nylon phase separation membranes that, despite their thin appearance, perform primarily as depth filters (Baker, 2004). In general, the surface pores are larger than the effective pore size. In low turbidity samples which are dominated by small particles, it can be expected that the membrane fouling will be dominated by pore-blocking. However, there is also likely to be varying degrees of surface cake formation depending on the amount of larger solids (Holdich et al., 2006).

In general, fouling models can be unified into the single differential equation (Bowen et al., 1995):

$$\frac{dJ}{dt} = -KJ(AJ)^{2-n}$$

Where K is a membrane-specific fouling constant and n is the blocking index which describes order of the fouling mechanism ranging from pore blocking to cake formation.

According to Bowen et al. (1995), filters undergoing complete pore-blocking fouling, the following equation describing the flux derived from the general fouling rate equation for $n=2$:

$$J = J_0 e^{-K_p t}$$

However, this complete-blocking scenario is rarely representative of reality. More often, the effective diameter of pores is gradually decreased as particles adhere to the inside of the pores. For this equation, the blocking index is $n=1.5$, yielding the standard blocking equation:

$$J = \frac{J_0^2}{(1 + 2A_{\text{eff}}K_s\sqrt{J_0t})^2}$$

Where A_{eff} is the effective area of the filter and K_s is the decrease in the cross-sectional area of the pores per volume of solution filtered.

Cake filtration occurs when buildup of particles on the membrane surface causes more particles to get trapped before even reaching the membrane. Under cake-formation dominated fouling conditions, $n=0$ and the equation describing the flux as a function of time is as follows:

$$J = \frac{J_0}{\sqrt{1 + J_0^2 K_c t}}$$

For micropore filters with the potential for simultaneous cake formation and pore blocking, the intermediate blocking formula for which $n=1$ is as follows:

$$J = \frac{J_0}{1 + J_0 K_p t}$$

The three principle factors that determine the primary mechanism of fouling are the filter type, pore size, and particle size distributions. Particle size has a significant impact on the fouling mechanism observed for a filter (Liu and Sun, 2012). The larger particles (greater than surface pore size) are expected to accrete on the surface of the membrane, forming a cake. When a solution has a wide distribution of particle sizes, this cake begins to form a pre-filter that traps fine particles and contributes to rapid fouling.

There are naturally advantages to each of these types of filter. On one hand, screen filtration ensures that particles are trapped on the surface where they are easily removed by backwashing. This characteristic makes them more consistent as an analytical tool because only the cake filtration fouling mechanism is expected to dominate; however, the resulting cake may be more easily disturbed if the filter is tilted during the analysis. Depth filters are more difficult to backwash; however, for the analytical process involving pore clogging, depth filtration is predicted to result in a more stable clogging behavior that would be less subject to perturbation if the filter is shaken or inverted.

According to Baker (2012) and Field et al. (1995) micropore filters clog more slowly at lower pressures. At higher flux, filters clog faster and more irreversibly. In one case, a flux of 50 L/m²/hr rendered the filter unusable in 20 hours while a flux of 30 L/m²/hr produced only very gradual fouling and ran for over 140 hours. Based on this trend, Field et al. introduced the concept of critical flux, below which only reversible fouling occurs. For these dead-end filter disks and similarly, biosand filters, this critical flux is very low—it must be low enough to allow re-suspension of the particles during filtration and provide insufficient energy to force these particles into pores. In cross-flow filtration, the critical flux can be much higher since the shear flow ensures that the particles remain in suspension rather than plugging pores and forming a cake.

For the analytical purposes of the filter clogging assay, a phase separation type depth filter with the lowest cost and smallest pore size should be operated at the highest practical pressure. The depth filter-type filter will result in the stable pore-blocking clogging mechanism to improve the ruggedness of the method. The cost must be minimized so that the assay is accessible in developing nation, so the cheaper

phase-separation type filters should be used. However, cost should be balanced against using a smaller pore size (0.2 micron rather than 0.45 micron), since smaller pore size will capture more particles and clog faster, likely reducing analysis time. Finally, higher pressures are desirable since they produce more permanent fouling and allow faster processing time; this is limited by the practical amount of weight that can be applied to the apparatus in order to drive the syringe since the user has to be able to lift the weight easily.

3 Methods

3.1 Preparation and Running of Biosand Filter Columns

Filter columns (Figure 6) were constructed from 3 foot sections of 7.65 ± 0.05 cm inner diameter (8.9 cm outer diameter) PVC pipe that were washed and a plastic barbed hose adapter (0.45 cm inner diameter) was inserted with a coarse plastic mesh screen 5 cm from the bottom (capped end of the pipe) and wrapped with Teflon tape. PVC caps and cement were used to close one end of the pipe. Four grades of limestone drain rock were added in order of increasing fineness up to 9.5 cm from the bottom according to the proportions outlined in Table 3.

Table 3: Distribution of grain sizes of limestone drain rock used in filter columns.

| Size interval (mm) | Surface dry mass (g) |
|--------------------|----------------------|
| 12.5-15.0 | 145 |
| 8.0-12.5 | 360 |
| 4.0-8.0 | 30 |
| 1.0-4.0 | 80 |

Filter columns were then filled with water and washed quartz sand sifted through a 30 mesh screen (see detailed particle analysis in Table 4) was added rapidly (so as to minimize fractionation) to a depth of 60 cm. A graduated cylinder was filled with water to 200 mL and then 100 mL of sand was added. The final volume was recorded to be 260 mL meaning that 40 mL of water were in the pore space of the sand, from this figure, the porosity of the sand was calculated to be 40%. 2600 mL of sand was added to each column. Latex hose was attached to the barbed hose adapter to bring the outlet height to 5 cm above the top of the sand. Tap water was run through the filters to test flow rates and wash out any residual small particles such as clays and organics. Eventually, the latex hose was replaced with PVC tubing since outdoor conditions caused the hose to crack. Prior to use, the filters were backwashed with dilute bleach solution to sterilize the filter and then rinsed out with 10 L of creek water. Despite the sterilization step, at one point, the PVC tubing was subject to colonization by biofilms on the inside of both the inlet and outlet.



Figure 6: Image of the completed filter columns and their location on Woods Creek in Lexington, VA under a bridge.

Table 4: The distribution of grain sizes of sand used in filter columns. It is estimated that the average particle size is 289 μ m the average pore size is 45 μ m.

| Size interval (mm) | Mass percent | Theoretical pore diameter (μ m) |
|--------------------|--------------|--------------------------------------|
| 0.500-0.595 | 20.91% | 78-92 |
| 0.250-0.500 | 68.77% | 39-78 |
| 0.125-0.250 | 10.00% | 20-39 |
| 0.063-0.125 | 0.23% | 10-20 |
| 0.000-0.063 | 0.09% | 0-10 |

Flow rates were measured upon commissioning and the permeability was calculated using Darcy's Law. Based on this flow rate, a 4.5 Watt, 5000 RPM, peristaltic pump with a flow rate of 70.6 \pm 3.9mL/min regardless of pumping height (up to 0.9 m) was used to bring water from Woods Creek to a reservoir for dispersion into the filter columns (Figure 6). The reservoir provides a degree of settling for the feed water to prevent over-loading of the filters with very high-turbidity water. Based on preliminary tests, the motor was found to heat up; in order to allow it to cool, it was programmed to run every other hour. The flow rate into each filter was set between 3 and 12mL/min via stopcocks that were adjusted so that the filters did not overflow as the effluent flow rate decreased. To avoid frost damage during the winter, a single filter was operated in the lab according to the same methods using water that was carried by bucket from the creek. When the flow rate in the filter decreased to impractically low levels it was harrowed as per the standard procedure (biosand.org). Harrowing was performed twice during the operation of filter 1 over the course of 6 months. After the last frost of the year, operation of filter 2 resumed and filter 1 was returned to its outdoor location. The filters were run as continuously as possible—it has been shown that the effectiveness of a continuously operated biosand filter can exceed that of an intermittently operated biosand filter (Young-Rojanschi and Madramootoo, 2014).

The influent water was drawn from Woods Creek in Lexington, VA, a small urban stream with a base flow of approximately 8 cfs. The intake was located under a bridge just downstream of an artificial weir. The presence of fecal indicator bacterium *E. coli* is of particular interest since the main city sewer line crosses through the creek at a number of locations and much of the watershed drains impervious

surfaces. Using the WHO sanitary inspection form for a protected spring as a proxy for sanitary inspection for Woods Creek, the score is in the 9-10 category—a very high risk. This is confirmed by the fact that *E. coli* concentrations have regularly been documented at concentrations ranging from 40 to 5057 CFUs/100mL near the sample location (W&L Biology 113 Lab, 2012). The location of the inlet under a bridge, while convenient for sheltering the filters may contribute to higher levels of *E. coli* since lower levels of sunlight are typically indicative of higher survival rates (Edberg et al., 2000).

3.2 IR of filter retentate

To evaluate the ability to detect biotic material using infrared spectroscopy an experiment with low turbidity (10 NTUs) creek water was performed to determine whether the ATR-FTIR was capable of detecting peaks that correspond to biotic compounds. First 250mL and 1000mL of the same creek water were passed through 0.45 μ m nitrocellulose filters; these filters were then dried in an oven at 50°C for 1 hour. A blank nitrocellulose filter was scanned as the background sample, followed by the other two filters. The samples were firmly clamped to the ATR crystal and the scan duration was approximately 2 minutes. Next, the absorption spectra were baseline corrected, normalized, and the blank spectrum was subtracted from the two sample spectra. As discussed later (section 4.2), the results of this test indicated insufficient sensitivity for detecting organics; however, inorganics such as clays and silicates were detected.

Following the filter clogging assay (section 3.4), certain representative 0.2 μ m nylon filters were examined via the same ATR-FTIR method. This was done to verify that the amount of inorganics in the filter effluent was much less when compared to the surface water inputs as well as to determine whether the absorption bands of the nylon filters interfered less with retentate.

3.3 Preliminary filter clogging experiment

Initial experiments to test the sensitivity of the FCA method made use of a 0.2 μ m filter (33mm diameter) with a 10mL plastic syringe. In order to ensure a stable flow rate, deionized water was run through the filter until the flow rate stabilized (three consecutive measurements within 1 standard deviation of each other). Then, the syringe was filled with 10mL of diluted surface water sample (procedure depicted in Figures 7 and 8). A constant force was applied by a vertically hanging bucket filled with a carefully measured mass of sand (total mass: 1.385 kg). This mass results in a pressure of 83 kPa (12 psi). The time it took to filter the water from the 9mL mark to the 1mL mark was measured and this volume (8mL) was divided by the time elapsed, resulting in the average flow rate for that volume. The average flow rate was plotted against the volume of sample filtered. Since the curve produced is essentially linear initially (for the first 50-100mL of sample filtered), the absolute value of the slope of linear least-squares fit to the flow rate measurements in this linear region was taken to be the clogging rate. The slope in this linear region was determined by comparing the R^2 for linear fits to the 10-50mL and 10-100mL regions and selecting the slope with greatest corresponding R^2 . This rate is indicative of the concentration of particles in the sample and is referred to as the regression-based clogging rate.

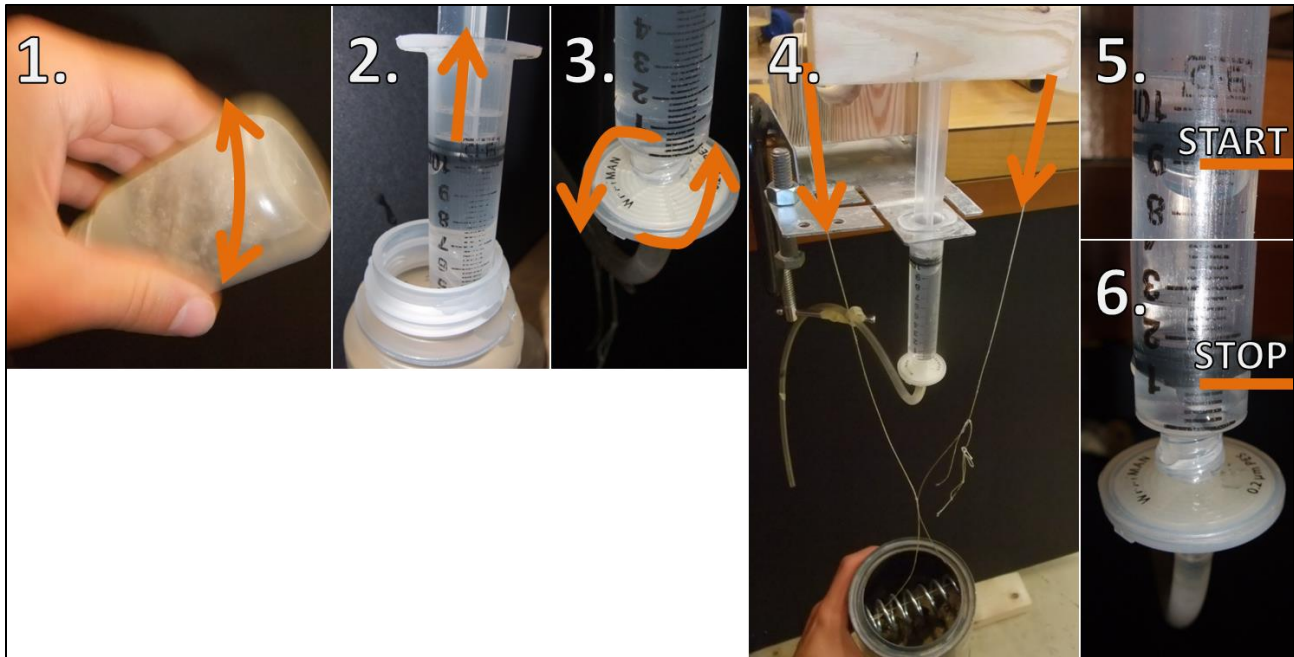


Figure 7: Photos outlining the procedure used for the filter clogging experiments. This process was repeated as many times as possible (until the flow rate became too slow to practically measure).

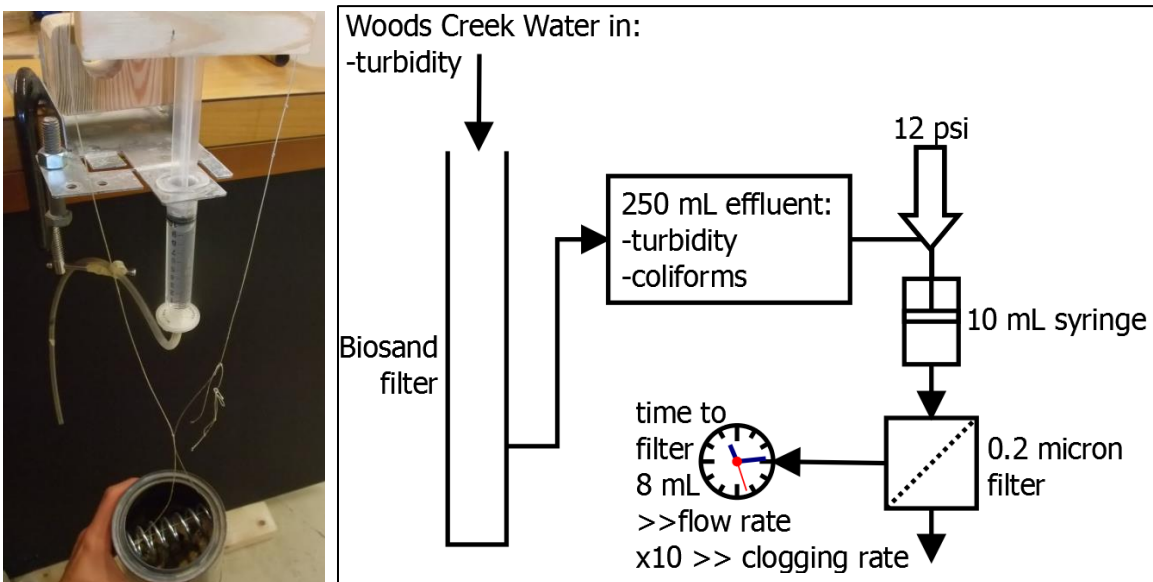


Figure 8: Experimental setup for the filter clogging experiments including a sample processing flow chart.

Since performing a regression is not practical in the field, the clogging rate would be calculated by subtracting the flow rate during the filtration of the second 10mL from the flow rate during the last 10mL, divided by the total volume filtered. This clogging rate, hereafter referred to as the endpoint-based clogging rate, is an estimate of the regression-based clogging rate. The regression and endpoint-based clogging rates were compared to test the hypothesis that they will be strongly linearly correlated so that the endpoint calculation can serve as a replacement for regression.

3.4 Correlation of filter clogging with bacterial counts and turbidity

After this initial proof of concept, the method remained largely unchanged; the key difference being that the samples were biosand filter effluent rather than diluted surface water. In addition to the clogging rate, two other parameters were measured: sample turbidity and *E. coli* and general coliform concentrations. The method was also further refined after uncovering potential sources of error. It was found that inverting or tipping the filter disk when it was removed to refill the syringe resulted in partial restoration of the permeability of the filter, so this was avoided. Furthermore, it was found that pressures of around 150 kPa resulted in partial restoration of permeability, meaning that filtrations in between the first and last 10mL could not be accelerated by applying more pressure. It is possible that the porous membrane has the potential to deform, allowing particles that are partially blocking pores to rearrange or pass through.

The turbidity of all sample influents and effluents was measured in Nephelometric Turbidity Units (NTUs) using a NeuLog turbidimeter that was shielded from the ambient light by a cardboard box. This \$200 instrument is typical of a low cost system that could be expected to be deployed by an NGO in a developing nation. The turbidimeter was calibrated using a 20 NTU standard solution of stabilized formazin (Hach StablCal®) and 3 serial dilutions and a 100 NTU standard solution of stabilized formazin diluted (see Appendix 9.1 for calibration data). For each sample, a separate DI water blank sample was analyzed in a polycarbonate cuvette. The values for the blank were subtracted from the filter influent and effluent sample measurements. For each sample, eight readings were taken, with a quarter turn of the cuvette between each reading. This was done to increase the accuracy and precision of these measurements by averaging out the variation in clarity of the cuvette or the detector, which can be significant at very low turbidity levels.

Coliscan® Membrane Filtration (MF) assays were performed on all samples to quantify the number of colony forming units of *E. coli* and general coliforms. For samples with clogging rates <0.5 mL/s/cm² per mL filtered, 200mL of sample were filtered undiluted. For clogging rates greater than or equal to $0.5 \leq 1$ mL/s/cm² per mL filtered, 150mL of sample were filtered. For clogging rates >1 mL/s/cm² per mL filtered, 50mL of sample were filtered diluted with DI water to 100mL. 1.5mL of Coliscan MF broth was pipetted onto pads in plastic petri dishes. The petri dishes were wrapped tightly in plastic wrap with a soaked paper towel and were incubated for approximately 24 hours at 37°C in an incubation oven. Upon removal from the oven after 1 day, the plates were opened and desiccated to prevent further growth and dry the colonies prior to scanning. The scanned images were used to count colonies of bacteria using image analysis software. Blue and purple colonies were identified as *E. coli* and red and pink colonies were identified as general coliforms. All bacteria counts were divided by the size of sample filtered and then multiplied by 100 convert them to units of CFUs/100mL. The total coliform parameter was calculated as the sum of the number of *E. coli* and general coliforms.

The correlations of both total coliform and *E. coli* concentrations with the linear clogging rate were assessed with linear regressions. Multivariate linear regressions were performed to assess how well turbidity alone and turbidity with the linear clogging rate explained both total coliform and *E. coli* concentrations. Finally, the clogging rate data were binned according to the four WHO water quality risk categories (assigned integers 1-4) based on the measured *E. coli* concentrations. Then 95, 90, and 85% confidence intervals were calculated for each average clogging rate to determine the level at which they are significantly different. A logarithmic fit was used to calculate the clogging rate values that correspond to the upper and lower limits of each risk factor along with the detection limit.

Finally, In order to verify that the solids in the biosand filter effluent that were clogging the membrane filters were primarily biotic, the Energy Dispersive Spectroscopy (EDS) instrument on an SEM in variable pressure mode was used to analyze two filters. A nylon filter that had been used in the clogging assay for a surface water sample from Woods Creek and 13.5 CFUs of *E. coli* per 100mL and turbidity of 2.35 NTUs was compared to a filter that had been used for the clogging assay for biosand effluent that had around 5.3 CFUs of *E.coli* per 100mL and turbidity of 0.08. Random sample sites on each filter were selected and imaged at 200x, 500x and 2100x magnification. It was found that, in some cases, deposits of calcium minerals had formed when the filter dried; areas with these deposits were avoided in the image analysis process.

3.5 Filter membrane regeneration

While already economical, the price of this analysis could be further decreased if filters could be used more than once. For this to be possible, the majority of the foulants need to be on the surface of the filter where they are easily washed off (Figure 9). After performing the filter clogging assay using a pair of filters, a backwash procedure was performed. Twice, 10mL of deionized water was passed through used filters that were dried out and the average flow rates were recorded. Then the filters were backwashed with DI water. Again, two 10mL forward filtrations were performed and average flow rates were recorded. To assess whether backwashing was more effective when the filter was still wet, the filter used for the assay of the March 1 sample from filter 1 was backwashed with 90mL in 10 mL intervals with the flow rate being checked each time.

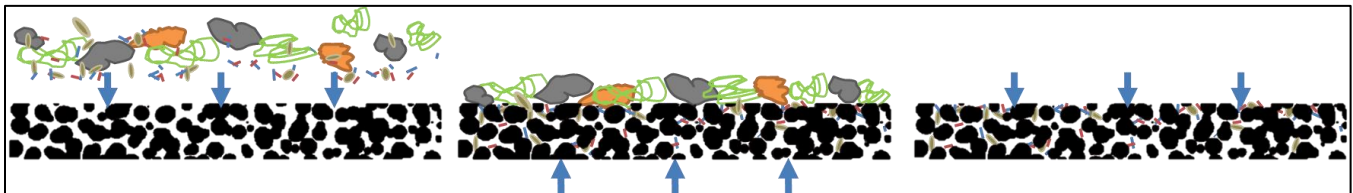


Figure 9: Diagram illustrating the effect of filter regeneration via backwashing in relation to reversible fouling (surface cake) and irreversible fouling (particles in the pores).

4 Results

4.1 Baseline filter properties

Upon commissioning, the average flow rate through the three columns was 15.98 ± 0.47 mL/min when the head pressure was at 4.5 cm based on the linear fit of flow rate data from all three columns (Figure 10).

The assumptions for Darcy's Law are satisfied:

- Laminar flow in saturated granular media: the Reynolds number (see below) remained less than 1 for all measured flow rates and the bed is devoid of air pockets.

Reynolds Number: $Re = \frac{\rho v_s D}{\mu}$; where v_s is the superficial velocity and D is the effective particle size.

- Under steady-state flow conditions: The filters were allowed to reach steady flow conditions before measurements were taken.
- A homogenous fluid: no significant thermal or chemical gradients existed in the tap water used for flow rate testing.

- Isothermal and incompressible: no temperature changes and water is negligibly compressible at room temperature.
- Neglecting the kinetic energy: the flow rate is very low, so kinetic energy is negligible.

The average flow rate listed above corresponds to a, head-independent, permeability of $0.082 \pm 0.020 \text{ mm}^2$, calculated from Darcy’s Law (Figure 11). A comparison of the average Darcy permeability for each filter supports the conclusion that the filters exhibit hydrodynamic uniformity since there is no significant difference in the average permeability for each column given a confidence interval of 95% (Figure 12)

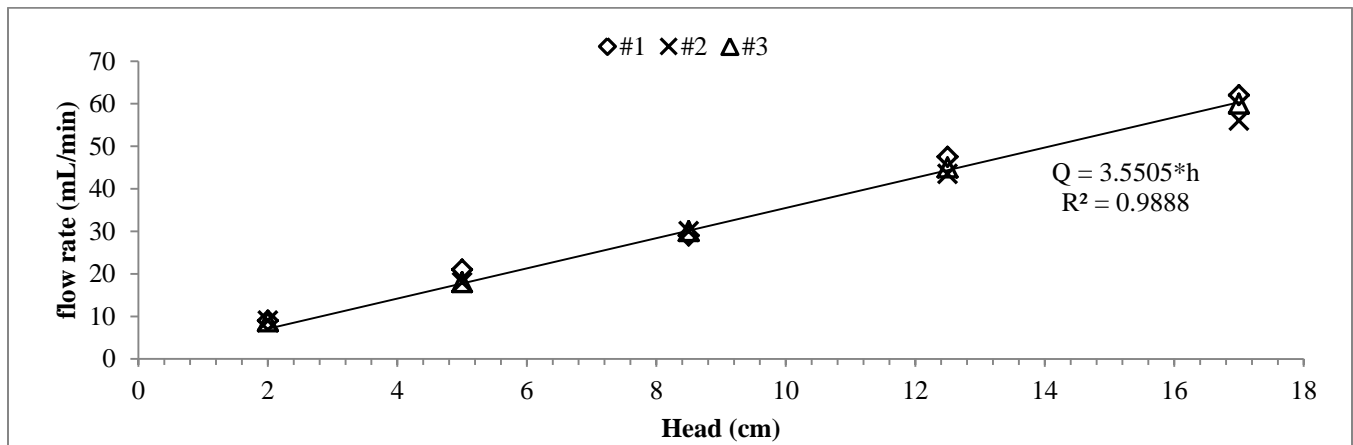


Figure 10: A plot of flow rate in each column versus the head pressure (the difference between the water level and the outlet height). The linear relationship is presented as an aggregate of the measurements for all three columns. The linearity matches our observation of a constant Darcy permeability.

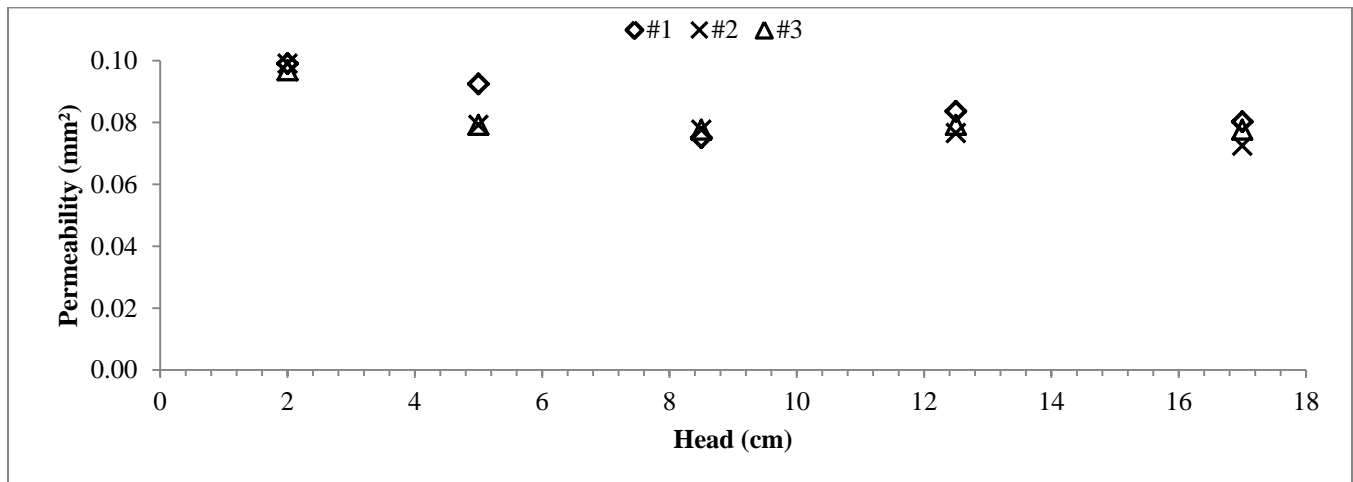


Figure 11: The Darcy permeability versus the head pressure. Only at 2 cm head is the permeability apparently slightly greater; over most of the range of operation, the permeability is independent of head.

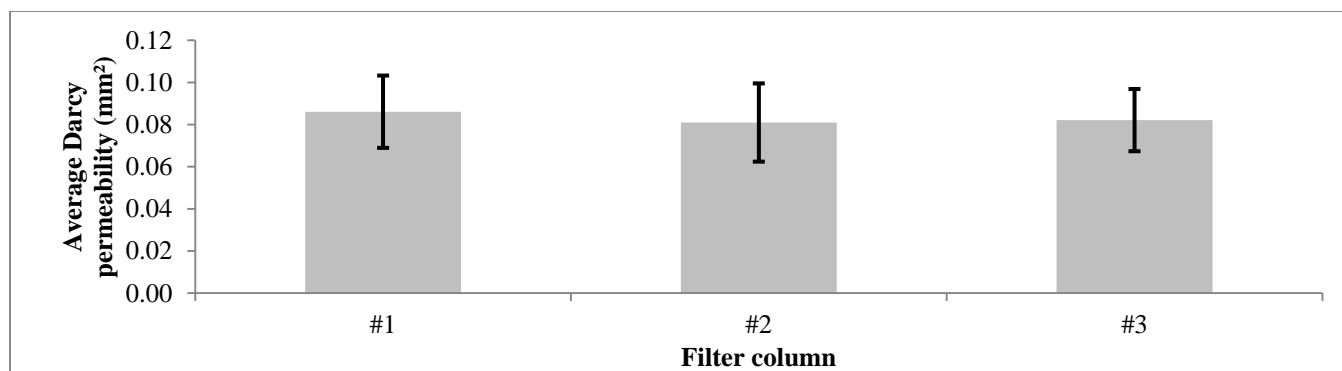


Figure 12: Comparison of the average permeability for each column; there are no significant differences, so the permeability is independent of column number.

4.2 IR Spectroscopy of filter retentate

It is important to note that after filtration, the membrane filters used on Woods Creek water showed visible coloration due to the solids collected on them, making visible recognition of the contamination possible. The blank nitrocellulose filter shows characteristic peaks at 1646 (asymmetric NO_2 stretch), 1278 (symmetric NO_2 stretch), 1087, 837 (N-O stretch), 1070 (C-O stretch), 834, and 745 cm^{-1} (NO_2 rock) (Figure 13). These absorption signals are increasingly obscured as the quantity of retentate on the filter increases (Figure 14). The strength of these absorptions varied with slight changes in the pressure applied to clamp the filter to the ATR crystal.

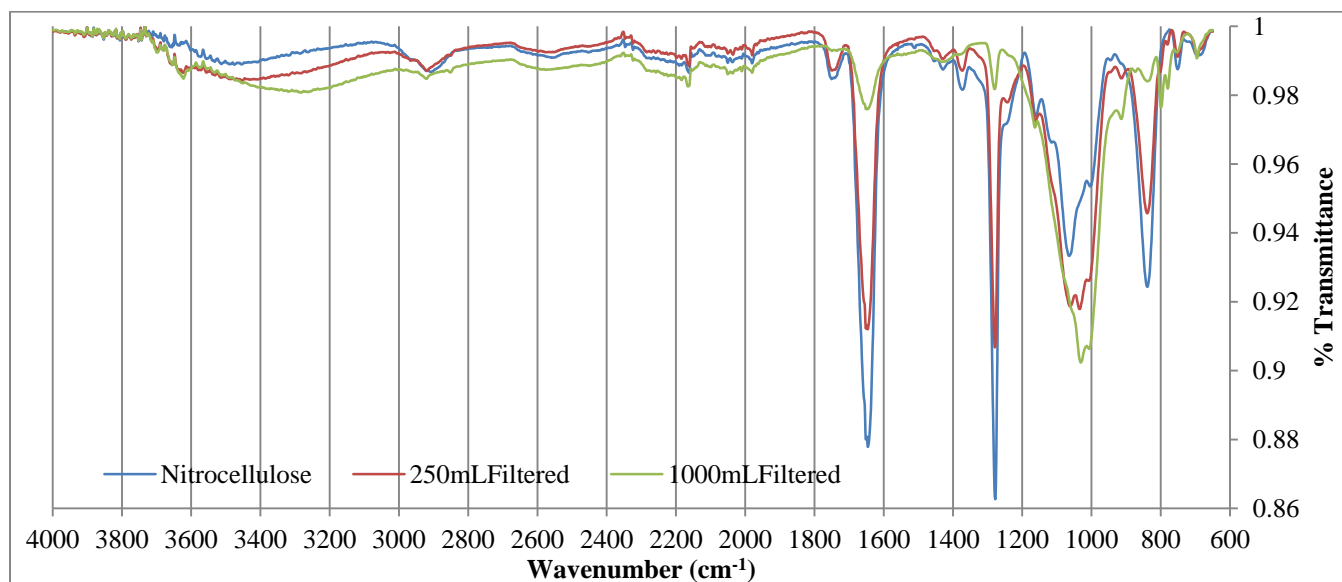


Figure 13: IR spectra of a blank nitrocellulose filter and filters with 250mL and 1000mL of creek water passed through them. The notable bands are those of clays and quartz. The nitro groups of the nitrocellulose also very prominent and may interfere with the detection of organics.

The weak signals at 3699 and 3621 cm^{-1} represent hydroxyl groups of clays (Djomgoue and Njopwouo, 2013). The signals at 1022, 1005, and 917 cm^{-1} correspond to the vibration of the Si-O bonds in silicates (Katti and Katti, 2006). Essentially, this spectrum shows the presence of clays and silicates; however, despite the clear presence of organic matter in the water, there were no bands clearly related to specific organic materials. If organics characteristic of bacteria were present in significant amounts, amide (1550

& 1650 cm^{-1}) and carbonyl ($1705\text{-}1745\text{ cm}^{-1}$) bands corresponding to proteins, saturated (2870 & 2956 cm^{-1}) and unsaturated (2850 & 2920 cm^{-1}) fatty acid bands, phosphate bands (1114 & 1222 cm^{-1}), and polysaccharide C-O band (1052 cm^{-1}) would be present (Schmitt and Flemming, 1998). The weak absorptions at 2852 and 2920 cm^{-1} corresponding to alkane C-H stretches differ slightly from the background filter signal at 2909 cm^{-1} ; however, the signal is too small to be significant even for this relatively dirty surface water sample for which organics are expected to be at a high concentration compared to filter effluent.

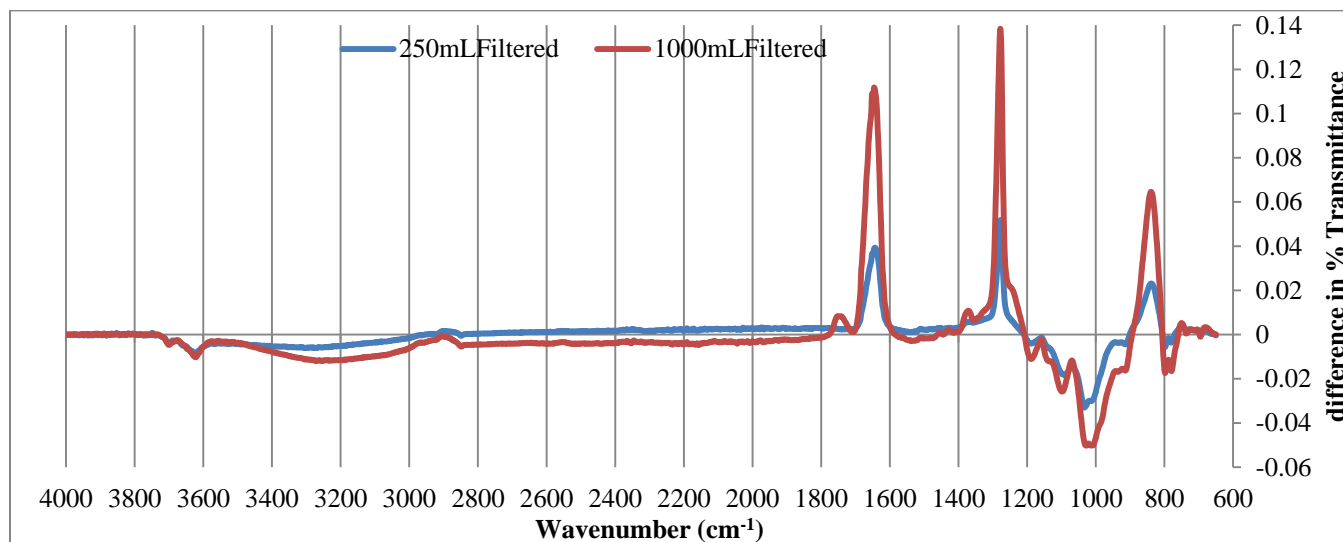


Figure 14: Spectra of the 250mL and 1000mL samples with the spectra for the blank nitrocellulose filters subtracted. Note that due to the material trapped on the filter, the NO_2 absorption is reduced. As a result, these spectra show positive nitro bands which obscure much of the fingerprint region.

4.3 Micropore filter flow rate assay

The proof of concept for the filter clogging assay compared the effectiveness of the clogging rate and turbidity in explaining the relative strength of dilutions of surface water. Overall, the turbidity decreased as the samples were diluted and the lowest measured turbidity was for the DI water. Higher strength samples produced greater clogging rates (Figure 15). It is worth noting that despite 8 replicate measurements of turbidity for each sample, the measured turbidity for the quarter dilution (5.495 NTUs) was indistinguishable from the measured turbidity for the half dilution (5.375 NTUs) (Figure 16). The filter clogging measurements showed a linear, decreasing trend in flow rate as more volume was passed through the filter. Though the initial flow rates varied (0.304 , 0.291 , 0.240 , and 0.250 mL/s) (Figure 15), the slopes determined both by regression and endpoints as described in the methods were clearly indistinguishable (Figure 17) and appeared to be independent of the initial flow rate.

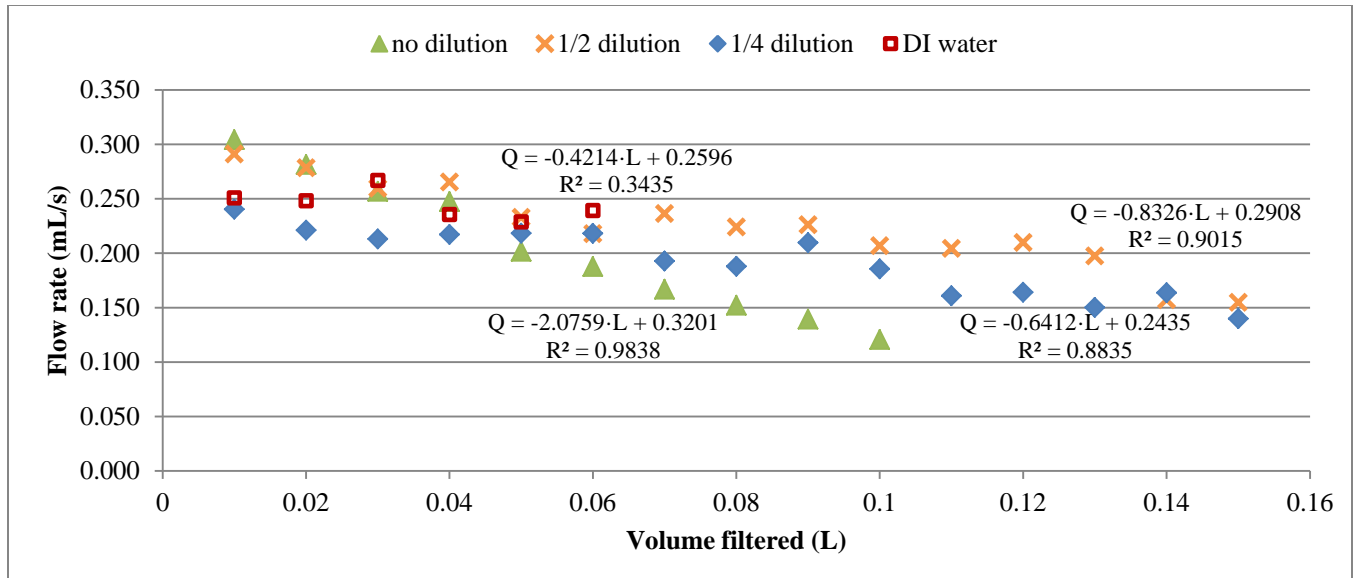


Figure 15: The change in flow rate through the filter for 3 strengths of a single sample of creek water and deionized water as a function of the volume of water filtered. As the filter is clogged the flow rate decreases. Since the flow rate cannot fall below zero, these linear fits are only valid for the range of data presented here; the flow rate will asymptotically approach zero.

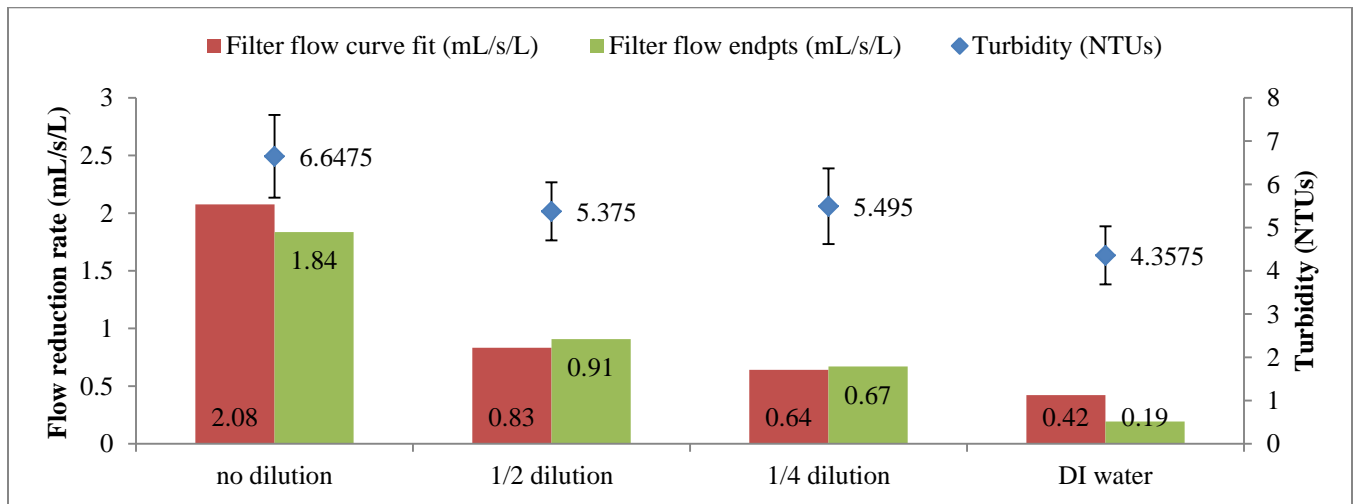


Figure 16: Comparison of indirect water quality measurement using a nephelometric turbidimeter in comparison to the filter flow rate reduction experiment. Note that the turbidity measurements are not significantly different from each other despite large differences in solution strength and the average for the 1/4 dilution was greater than that of the 1/2 dilution contrary to what is expected. Error bars represent the 95% confidence interval.

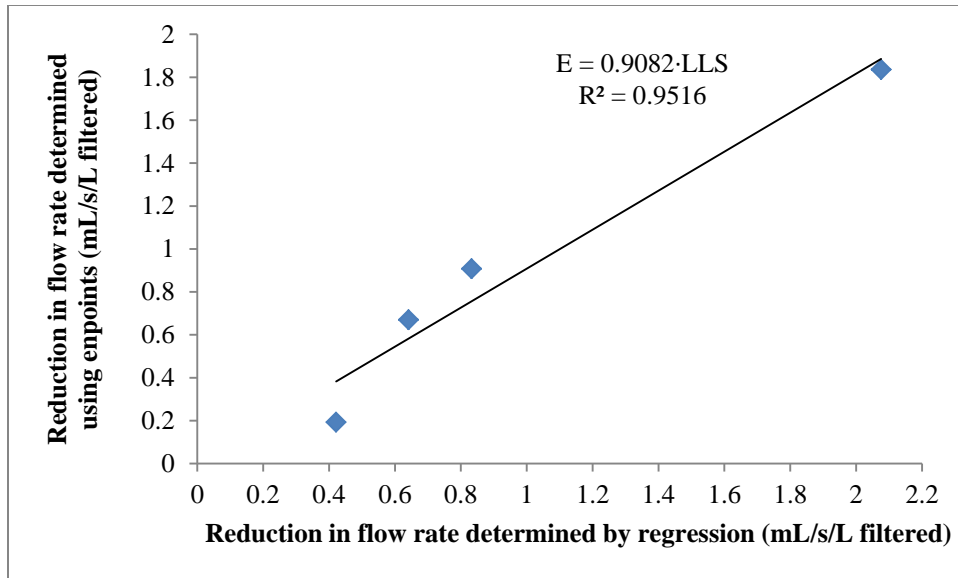


Figure 17: Linear correlation between the reduction in flow rate determined via linear regression and the reduction in flow rate determined using first and last filtration time (endpoint method).

After the proof of concept, data such as those shown in Figure 18 were collected, a total of 22 filter clogging tests were performed. The slopes determined by regression for each sample are included in Appendix 9.4.

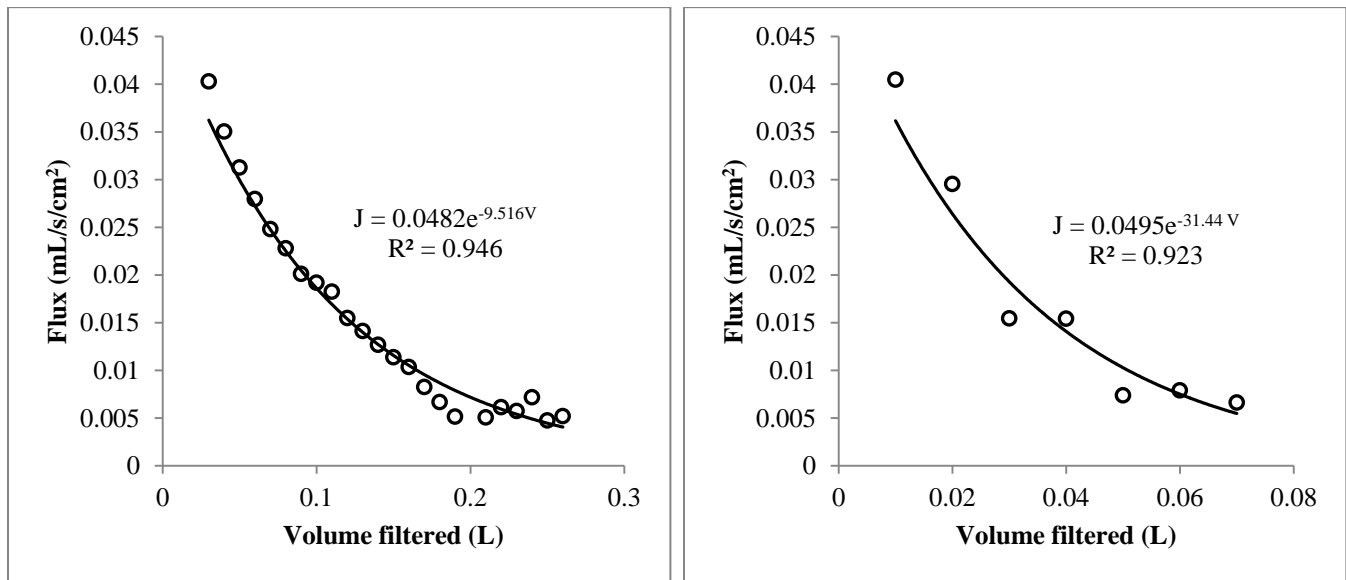


Figure 18: Flow rate data for the no dilution and half dilution experiments with exponential curves fit. An exponential model accurately describes the clogging behavior of the filter in terms of volume.

One of the objectives of the filter clogging assay experiment was to verify that individual filter disks yielded repeatable results for the same sample. Replicate measurements were performed for two of the samples. For the sample taken on February 4th from filter 1, the clogging rates determined by linear regression were 0.351, 0.373, 0.362 mL/s/cm² per mL filtered, corresponding to a relative standard deviation (RSD) of 3%. For the sample collected on February 12th from filter 1, the clogging rates

determined by linear regression were 0.803 and 0.870 mL/s/cm² per mL filtered, corresponding to a RSD of 6%.

As with the proof of concept, it was critical to demonstrate that the relationship between the regression method and the endpoint method for determining the slope is sufficiently linear so that regression does not have to be performed in the field. The correlation between the clogging rates determined by the two methods is presented in Figure 19. The greater volume (100 mL) of sample filtered produced a much more accurate representation of the actual clogging rate compared with the smaller volume (50 mL only)

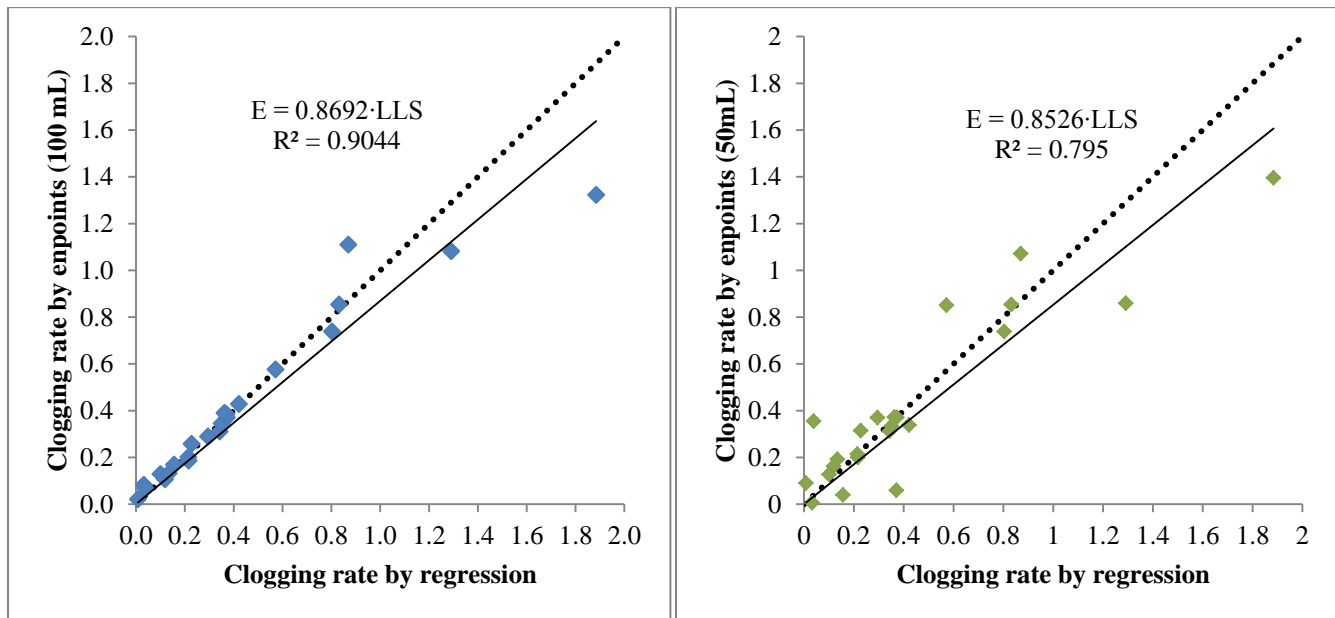


Figure 19: (left) Comparison of the clogging rate determined using least-squares fit to the linear region of the flux-volume filtered data with the clogging rate determined by calculating the slope between the initial flux and the final flux (after filtering either 100mL for relatively clean sample or 50mL for a few very dirty samples). (right) The same comparison of least-squares fit to the linear region of the flux-volume filtered data to the clogging rate determined by calculating the slope between the initial flux and the flux after filtering 50mL of sample.

To summarize, the proof of concept gave initial confirmation that a measurement of filter clogging rate is an improvement over turbidity for measuring the amount of solids in surface water and the clogging rate as determined by endpoints was sufficiently linearly correlated to the clogging rate determined by regression. This prompted the completion of 22 filter clogging assays (with some replicates) for 14 samples from the biosand filter, 1 deionized water blank, and 2 samples from Woods Creek. The results of these assays showed similarly strong correlations between the regression-based and endpoint-based clogging rates calculated from the flow rate data the first 100 mL of sample filtered.

4.4 Micropore filters clogged by bacteria or turbidity

In order for the filter clogging assay (FCA) to be effective, the clogging should be minimally effected by large particles such as algae, detritus, silt, and clay. To verify this, the turbidity of biosand filter effluent was measured and individual membrane filters used in the FCA were examined using IR and SEM instruments.

As with any micropore filter, removal of solids is dependent on the effective pore size. Naturally, some sources of turbidity such as clays and colloids are small enough to pass through the filter. Figure 20 presents the influent and effluent turbidity measurements for one filter over the course of 4 months. The partial breakthrough of turbidity-causing particles is evident from the least-squares fit presented in Figure 22. Increases in influent turbidity generally resulted slight increases in effluent turbidity; however, there are some outliers due to confounding factors such as biofilm growth on the outflow tube, delay in the breakthrough of turbidity, and variation in flowrates. Removal efficiency (Figure 21) ranged from 65% to 99%. A complete analysis of the factors influencing biosand filter performance in terms of turbidity is outside of the scope of this work.

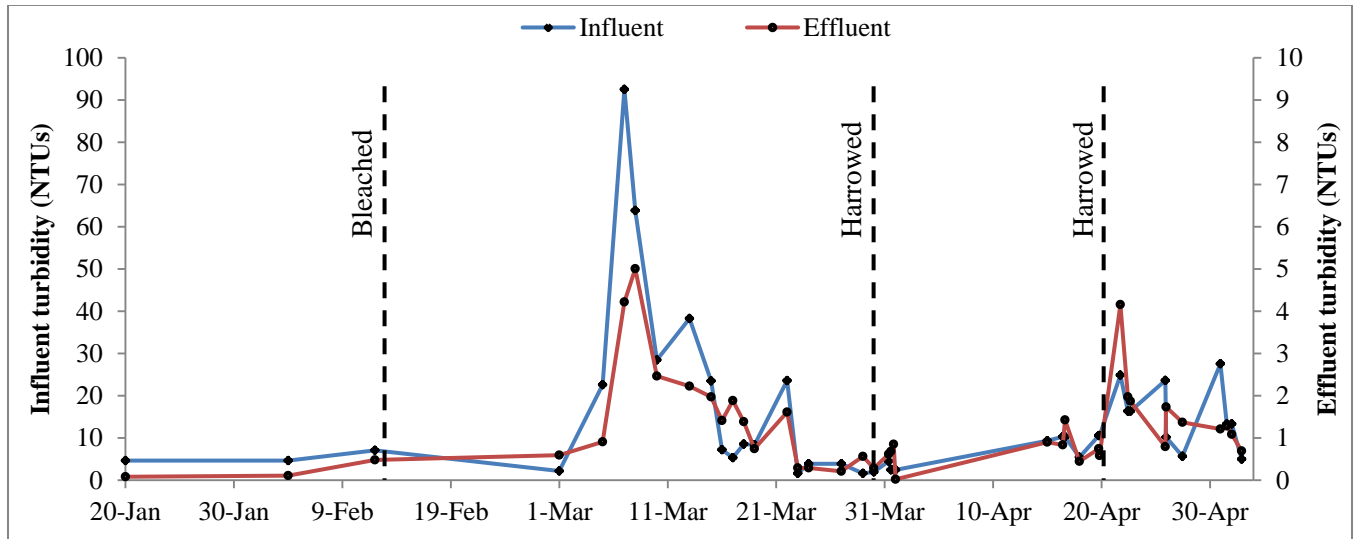


Figure 20: The influent and effluent turbidity measurements taken over the course of 4 months of filter operation. Cleaning events are marked with dashed lines. Note that the influent and effluent values are scaled to different axes to aid in interpretation.

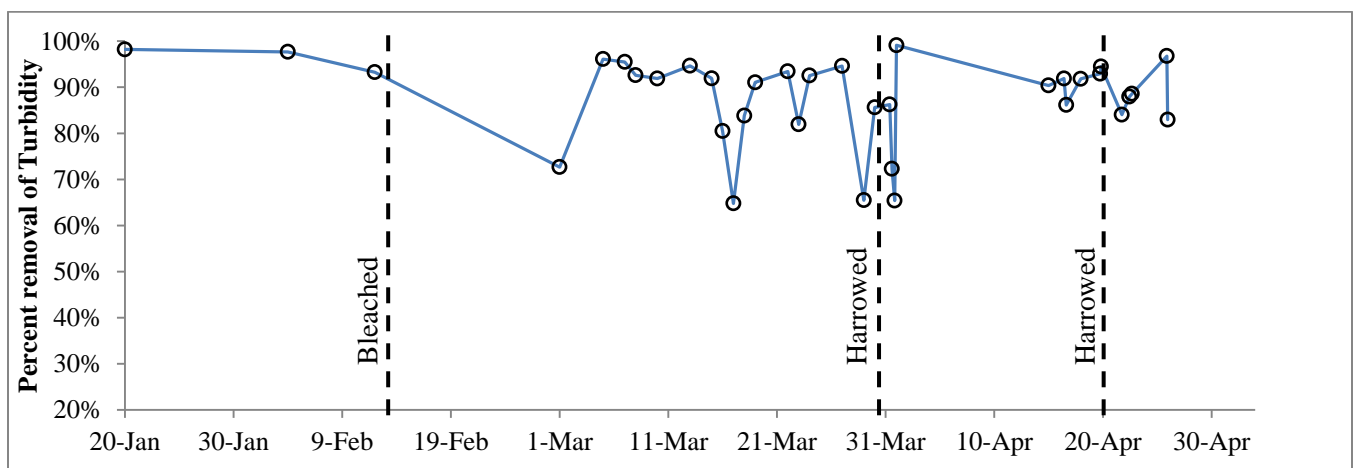


Figure 21: Percent removal of turbidity by the biosand filter. Cleaning events are marked with dashed lines

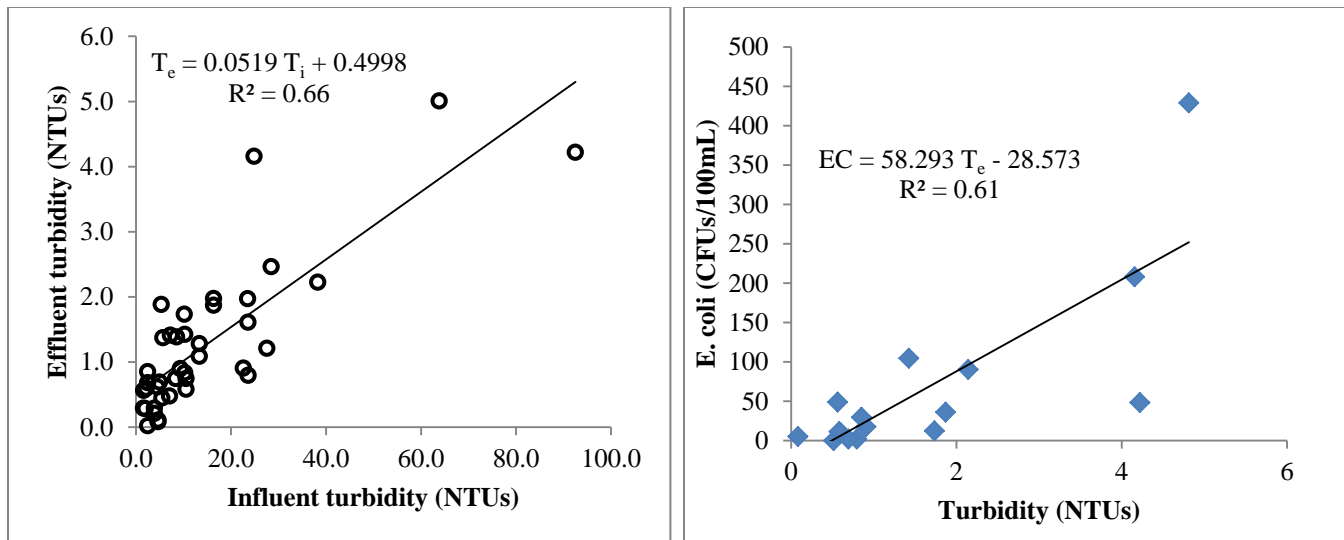


Figure 22: (left) the moderate correlation between the influent and effluent turbidities indicate that there is some breakthrough of silts and colloids; however, this correlation does not translate into an ability to determine the bacterial quality of the effluent—(right) there is a weak correlation (linear $R^2 = 0.61$) between *E. coli* concentrations and effluent turbidity.

After performing the filter clogging assay, two $0.2\mu\text{m}$ nylon filters were examined via the same ATR-FTIR method described in section 3.2. These peaks correspond to the bonds in the nylon that absorb strongly in the IR—the alkane C-H (2936, 2860), 3296, ketone stretch 1633, amide 1538. The spectrum of BSF effluent filter minus the average of the two blank spectra yields a spectrum that is very similar to the blank difference spectrum. The spectrum of the Woods Creek surface water filter clearly deviates from the previous two spectra with broad peaks corresponding to clays and silicates (areas indicated in Figure 23). This reinforces the conclusion that the clogging of the filters is not due to inorganic solids that are relatively abundant in surface water, but not in biosand filter effluent. As seen in Figure 23 the spectrum of a blank nylon filter results in characteristic peaks.

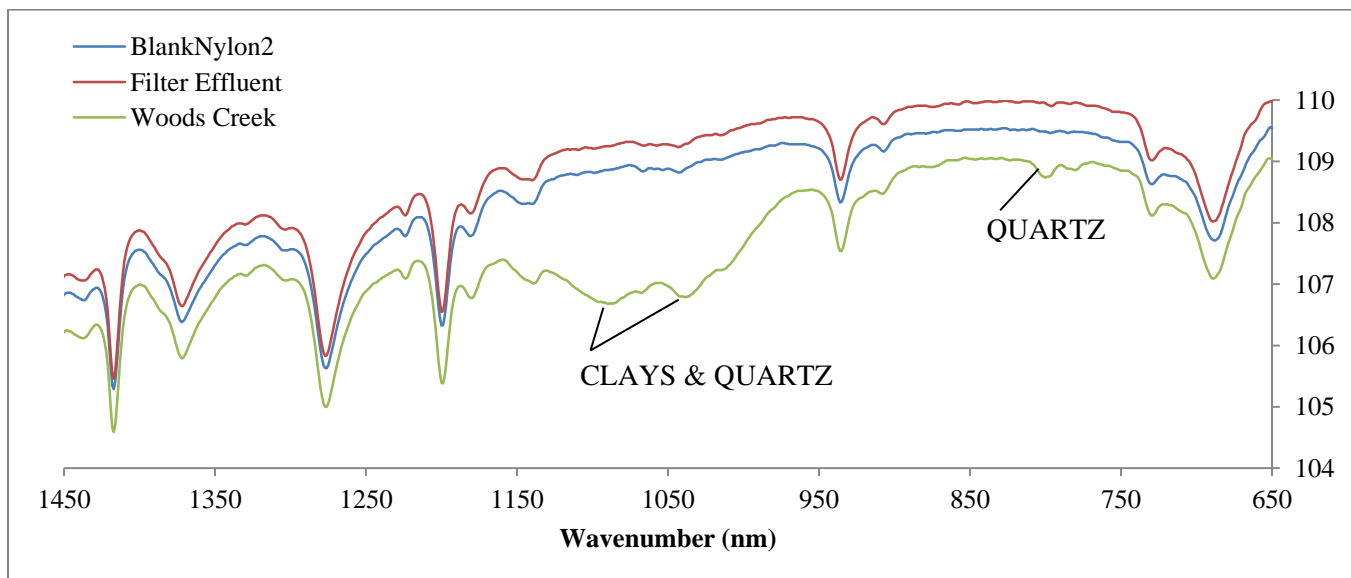


Figure 23: Infrared spectra of three nylon filters: a blank, a filter used on 140mL of Biosand effluent, and a filter used on 260mL of Woods Creek water. Full spectrum is available in Appendix 9.2.

SEM-EDS analyses (see Appendix 9.3) were used to verify the differences in cause of fouling between the same two filters examined using FTIR. At the 200 times magnification level, the respective intensities of the silicon and calcium signals for the Woods Creek sample were 7.02 and 1.68 times that for the biosand effluent sample. A similar, but weaker contrast was observed at the 500 times magnification level.

4.5 Bacterial cultures

A complete list of bacterial culture results is available in Appendix 9.4. *E. coli* concentrations in the filter effluent ranged from 2 to 429 CFUs/100mL. General coliform concentrations ranged from 27 to 472 CFUs/100mL (Figure 24). For most of the samples, general coliform concentrations were greater than *E. coli* concentrations. The relationship between the two types of coliforms is presented in Figure 24, the fact that they are poorly correlated gives a preliminary indication that the clogging rate may predict total coliform concentrations better than *E. coli* concentrations alone, since both general coliforms and *E. coli* are trapped on the filter.

Two outlier samples (corresponding to 5 clogging rate data points) were analyzed during a time when the filter was moved from outdoors to indoors and the outlet was colonized by bacteria, resulting in water that contained between 1000 and 2000 CFUs/100mL of *E. coli*. These high concentrations were detected by the filter clogging assay; however, they were too high to be reliably counted using the Coliscan plates. These results prompted a recommissioning of the filter by backwashing the filter with chlorine bleach. These outliers were not included in the linear correlations presented in the following section. However, they were included in the binned values used to describe the WHO risk category (Figure 25, Section 4.6) since they represented a significantly high level of contamination that prompted immediate corrective action as expected for a very high risk sample.

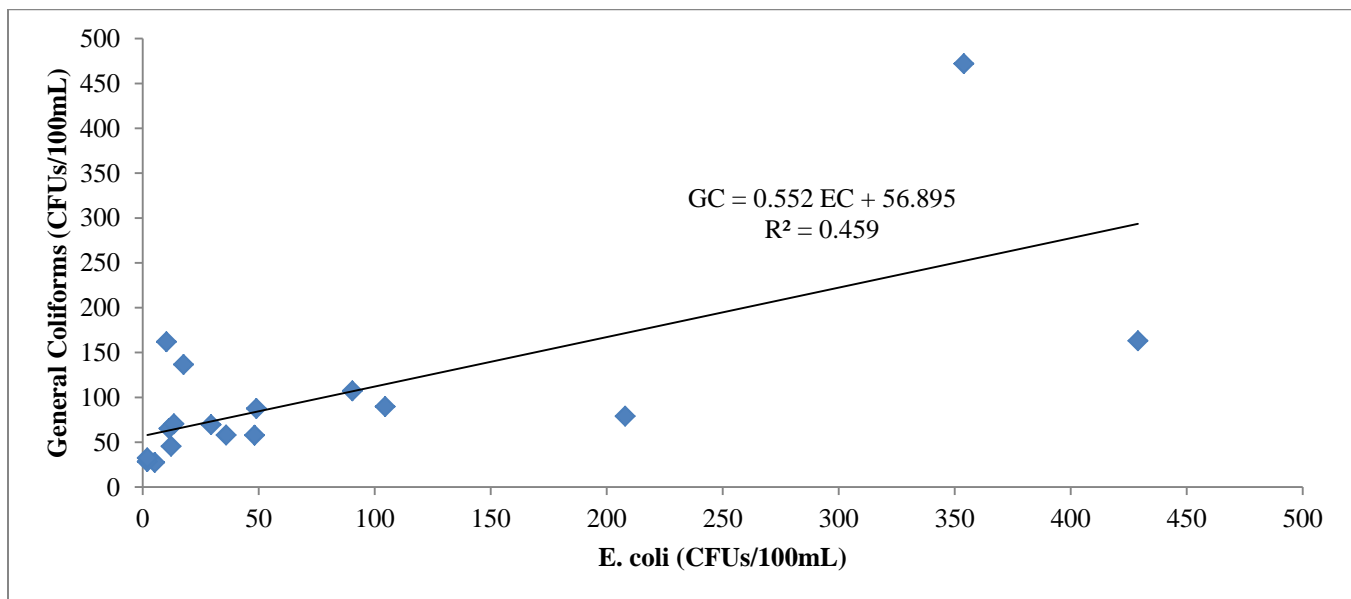


Figure 24: The weak linear correlation between the concentration of *E. coli* and the concentration of general coliforms.

4.6 Model for coliforms and pathogenic risk

Linear regression models using turbidity and/or clogging rate parameters to explain either total coliforms or *E. coli* concentration were compared to determine the best model for the two bacterial

parameters (Table 5). All models used 17 of the 22 data points, excluding the outliers described in section 4.5. The clogging factor is more effective than turbidity at explaining concentrations of both total coliforms and *E. coli*. It is also more effective at explaining total coliform concentrations than *E. coli* concentrations. The regression-based clogging factor was generally more effective at explaining the bacterial concentrations than the endpoint-based clogging factor. Turbidity was useful for increasing the accuracy of the clogging-rate models of bacterial concentration, especially when the endpoint-based clogging factor was used. The detection limit of 49 CFUs/100mL for the endpoint-based clogging rate predicting *E. coli* is still too high to discern between medium risk (<10 CFUs/100mL) and high risk (>10 CFUs/100mL) samples.

Table 5: Intercept, coefficients, standard error, goodness of fit, significance level, and detection limit for linear least squares models explaining either total coliform or *E. coli* concentrations using turbidity and/or clogging rate.

| Independent variable | Regressors | Intercept | Standard Error | Clogging rate coefficient | Standard Error | Turbidity coefficient | Standard Error | R ² | Significance | Detection limit (CFUs per 100mL) |
|----------------------|---------------------------------------|-----------|----------------|---------------------------|----------------|-----------------------|----------------|----------------|--------------|----------------------------------|
| Total coliforms | Turbidity | 84.70 | 31.24 | --- | --- | 33.39 | 5.10 | 0.74 | 9.2E-06 | 178 |
| <i>E. coli</i> | Turbidity | 35.27 | 26.56 | --- | --- | 16.03 | 4.33 | 0.48 | 2.1E-03 | 115 |
| Total coliforms | Turbidity, Clogging rate (regression) | 12.61 | 20.82 | 390.79 | 64.79 | 2.44 | 5.85 | 0.93 | 1.0E-08 | 75 |
| <i>E. coli</i> | Turbidity, Clogging rate (regression) | -29.50 | 13.69 | 354.75 | 42.61 | -12.11 | 3.85 | 0.91 | 4.0E-08 | 41 |
| Total coliforms | Turbidity, Clogging rate (endpoints) | 3.46 | 22.56 | 385.41 | 72.84 | 13.11 | 5.02 | 0.93 | 3.6E-08 | 71 |
| <i>E. coli</i> | Turbidity, Clogging rate (endpoints) | -39.30 | 18.74 | 348.79 | 56.72 | -3.00 | 3.87 | 0.86 | 1.1E-06 | 56 |
| Total coliforms | Clogging rate (regression) | 10.98 | 19.24 | 413.52 | 30.05 | --- | --- | 0.93 | 6.5E-10 | 69 |
| <i>E. coli</i> | Clogging rate (regression) | -16.33 | 16.46 | 236.98 | 25.70 | --- | --- | 0.85 | 1.4E-07 | 49 |
| Total coliforms | Clogging rate (endpoints) | -11.76 | 30.60 | 521.13 | 58.26 | --- | --- | 0.84 | 2.1E-07 | 92 |
| <i>E. coli</i> | Clogging rate (endpoints) | -35.08 | 17.69 | 313.76 | 33.67 | --- | --- | 0.85 | 1.3E-07 | 53 |

An alternative model, using the average clogging rates corresponding to the *E. coli*-based WHO risk categories is presented in Figure 25. The average clogging rate for the low risk category was significantly lower than that for the medium risk category at the 90% significance level ($p=0.10$). The medium and high as well as the high and very high risk categories were significantly different at the 95% significance level with $p=0.05$ and $p=0.02$ respectively. As expected the averages of *E. coli* concentrations that were binned according to each risk category, followed a logarithmic trend (Figure 25).

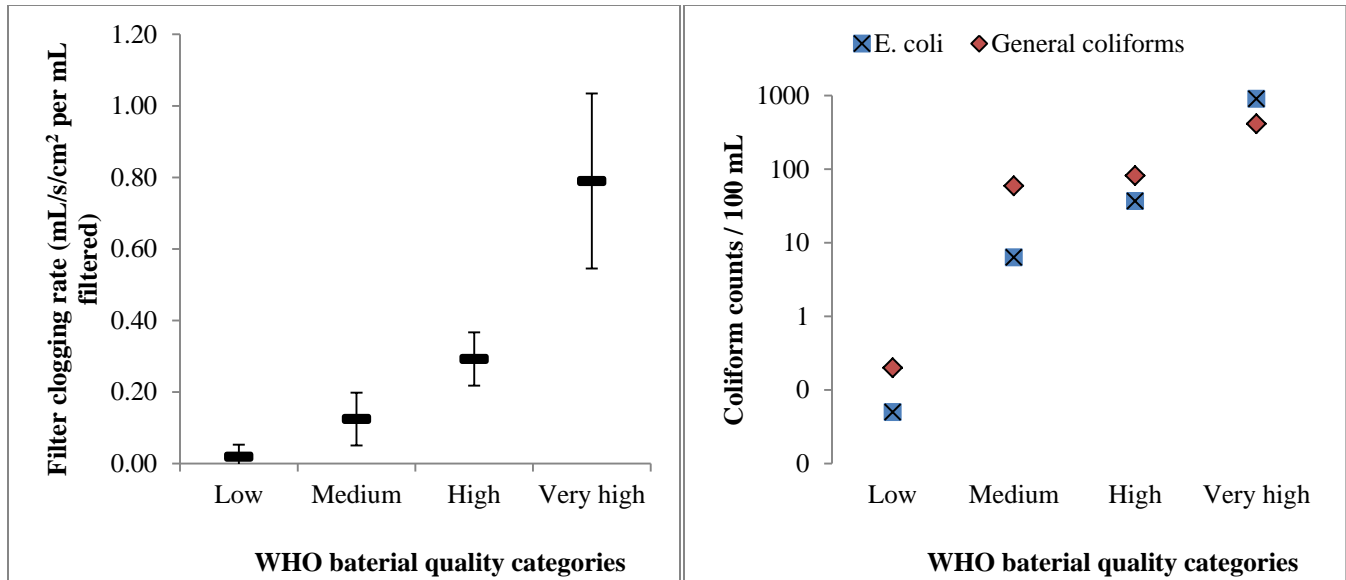


Figure 25: (left) plot of the average clogging rate for each sample classed using *E. coli* concentration according to the WHO risk categories along with corresponding 80% confidence intervals calculated using the t-distribution, (right) comparison of the average CFUs/100mL of *E. coli* and general coliforms for each sample classed according to their WHO-defined risk category.

4.7 Micropore filter regeneration

The first filter regeneration experiment investigated backwashing the filters after they had dried for 2-3 weeks. Even after drying, the percent of the original flux increased by 32-55%. A subsequent backwash treatment with 10mL of DI water resulted in 8-15% recovery to around 80% of the original flux (Figure 26).

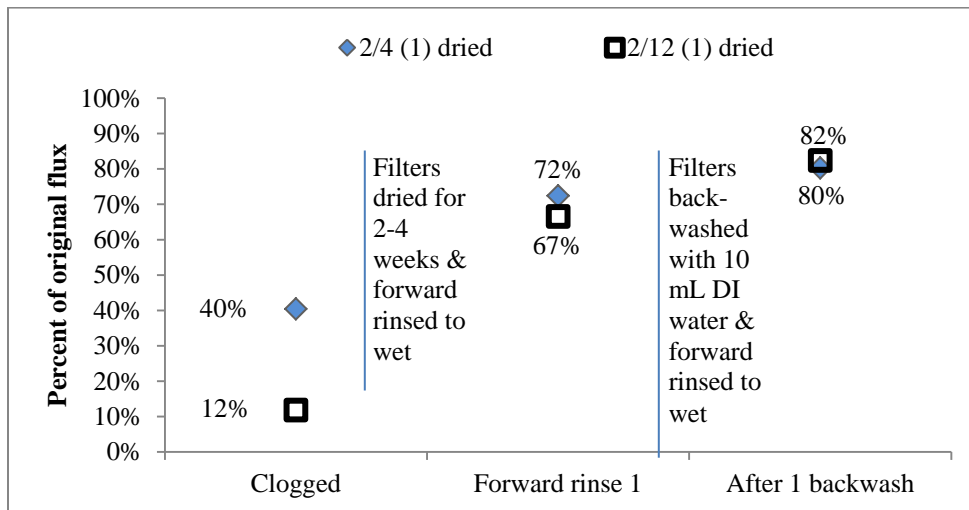


Figure 26: Plots of the recovery of flux after drying and backwashing treatments. Note that for all backwashing scenarios there some permanent fouling is expected as the recovery asymptotically approaches a value less than 100%

A brief investigation of the ability of the flux to recover after backwashing the filters while they were still wet was also performed. Figure 27 illustrates that the recovery of the filter as a percentage of its original flux converges on only 50% after 90mL of backwash. This seems to indicate that there is a substantial amount of irreversible fouling due to small particles and bacteria entering the pores.

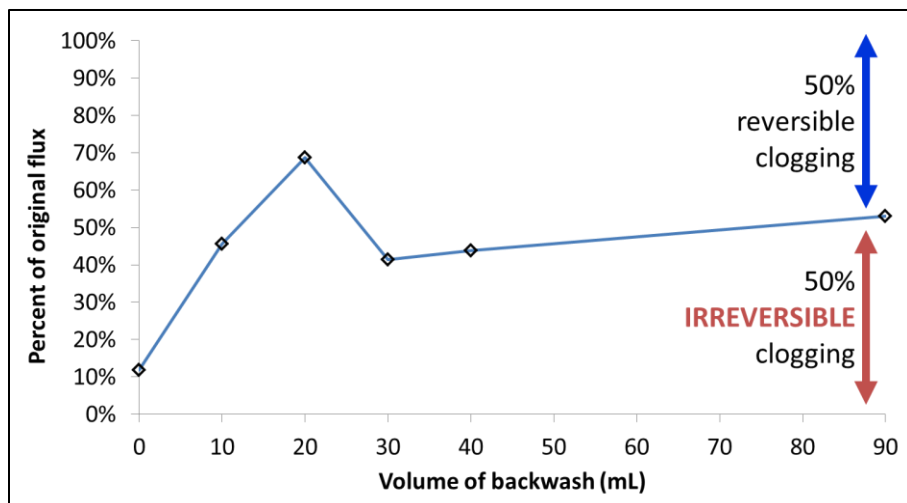


Figure 27: Recovery of flux as a function of the volume of backwash used.

5 Discussion

5.1 IR spectroscopy of micropore filter retentate

The IR spectra did not provide sufficient sensitivity to detect organic compounds in these water samples. The signal due to the retentate was often heavily obscured by the absorptions due to the nitro groups of the nitrocellulose filter. The sensitivity might be able to be improved by using polypropylene filters instead since polypropylene only contains saturated alkane groups (Howe et al., 2002). The only bands that were identifiable corresponded to clays and silicate minerals. The work done in identifying the clay and quartz absorption bands did lay the foundation for identifying inorganic foulants on the nylon filters used later in this study. The absence of any clear organic functional group absorptions was a clear indication that a simple single-band IR instrument for estimating bacterial concentrations would be difficult to construct and likely too expensive. Furthermore, the filters needed to be well dried prior to analysis since water absorbs heavily in the infrared range. However, after filtering large quantities of water, coloration appeared on the filter, indicating the formation of a cake on the membrane surface. In recognizing that at a constant head, the flow rate through a micropore filter will decrease, it was realized that a filter that traps all solids serves as a proxy for total suspended solids.

5.2 Proof of concept for the filter clogging assay

As seen in figure 16, section 4.3, the turbidity was a less useful predictor of the strength of a solution and therefore likely less useful in determining the quantity of contaminants in the water. The demonstrated sensitivity of the filter clogging method is likely even more essential in low turbidity filter effluent where turbidity differences can be very slight. Also, the rate of reduction in flow rate determined by regression corresponded well with the rate determined using the endpoints ($R^2 = 0.95$). In order to be practical in the field, the proposed assay cannot rely on the computationally more intense regression of many data points as a means of determining the clogging rate, it is important that the endpoint method agrees well with the regression method.

A major concern was that the micropore filters are not uniform enough to provide consistent results. Some non-uniformity is a probable explanation for the measured variability in the initial flow rates through each of the three micropore filters used (0.304, 0.291, 0.24mL/s). While these variable starting

points did not appear to affect the slope of the curve, multiple filters needed to be compared in the full experiment for the same sample to verify repeatability.

The proof of concept supports that the filter clogging assay would be more sensitive than turbidity for determining the amount of contaminants in a low turbidity water sample. Also, the suitability of this method for field applications was confirmed by showing that the clogging rate determined by the slope between the initial time and final time was sufficiently correlated with the clogging rate determined by regression (Figure 19). This proof of concept exposed three variables which need to be accounted for in the full experiment. Firstly, the optimal volume of sample that should be filtered during the assay had to be determined so as to maintain accuracy and remain in the linear region. While the flow rate decreased linearly, it is expected that the flow rate will begin to asymptotically approach zero. This should be confirmed over the entire range of samples in order to determine the optimal volume of sample to be used in the clogging assay. Secondly, the clear discoloration of the micropore filters served as a clear indication that suspended inorganic solids were largely responsible for the clogging; the full experiment needed to include verification that suspended clays and silts were not responsible for the majority of clogging caused by biosand effluent. Lastly, the variability in the clean water flux of individual micropore filter disks was sufficient to merit an investigation of the consistency of the results for a single sample using multiple filters.

5.3 Micropore filter fouling mechanism in relation to assay

The three principle clogging rate equations discussed in section 2.6 were fit to those assays for which a full clogging profile had been developed. The regressions were performed for the four equations modeling the mechanisms discussed in section 2.6 and R^2 values for each regression were compared; the model with the highest R^2 was selected. In cases where the data collected did not extend into the non-linear region of the clogging rate curve, the identification of the clogging mechanism for the micropore filter was subject to a greater degree of uncertainty. Nonetheless, it was found that the majority of the filters clogged according to the standard pore blocking equation:

$$J = \frac{J_0^2}{(1 + 2A_{\text{eff}}K_s\sqrt{J_0t})^2}$$

This indicates that the dominant mechanism involved a gradual reduction in the pore diameter due to the accretion of small particles. This makes sense—the effluent from a biosand filter should mostly contain 1-5 μm particles that enter the larger surface pores of the membrane and partially block them. SEM-EDS analyses (Appendix 9.3) supported this assumption; the micropore filter used for the Woods Creek sample contained substantially more silicon and calcium-based minerals of much larger size compared with the filter used for the biosand effluent. This clearly supports the hypothesis that large cake-forming solids are mostly absent in the BSF effluent.

Two examples of filters that underwent standard blocking are presented in Figure 28. A clear deviation from the standard blocking model was observed for the sample of BSF effluent taken on 2/12, when the outlet had been colonized by bacteria and concentrations were very high. In this case, cake filtration was observed. One possible explanation for this is that the bacteria accumulated fast enough to block the pores at the surface and begin forming a cake. The Woods Creek sample taken on 4/25 produced intermediate blocking conditions. This is likely due to the combination of small and large particles with some forming a cake that allowed small particles through to partially block pores.

Linking the fouling mechanisms to the turbidity and bacterial concentrations in each sample reinforces the earlier hypothesis that much of the clogging is due to small particles such as bacteria which enter into the pores of the filter. Pore blocking is a very stable form of fouling that is irreversible. While this means that the filter cannot be reused, it does ensure that the progress of fouling is more steady and is not disrupted by dislodgement of a cake.

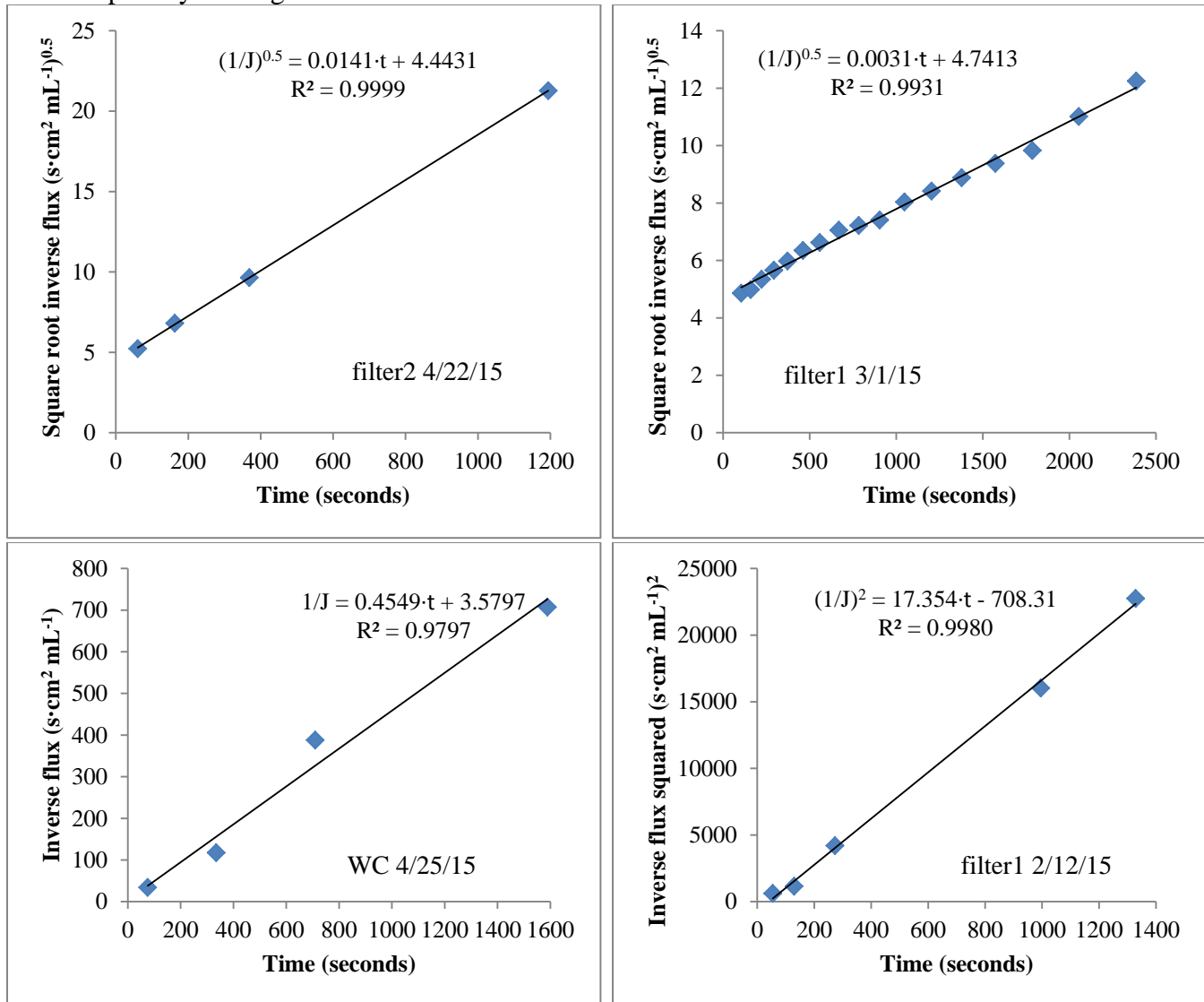


Figure 28: Least-squares lines describing the blocking mechanism model that has the highest R^2 out of the 4 models presented in section 2.6. Top left: standard blocking, 592 total coliforms, 4.81 NTUs. Top right: standard blocking, 172 total coliforms, 0.60 NTUs. Bottom left: intermediate blocking, 826 total coliforms, 23.62 NTUs. Bottom right: cake filtration, 3191 total coliforms, 0.48 NTUs.

5.4 Accuracy of the micropore filter clogging assay

While general coliforms are typically measured as part of a bacterial culture, there are many naturally occurring coliforms in soil and water. *E. coli* are exclusively generated in animal guts, enter the environment through feces, and therefore, are a much better indicator of potential contamination with enteric pathogens (Edberg et al., 2000). Though the filter clogging assay is not able to distinguish between general coliforms and *E. coli*, a strong correlation between the clogging rate, turbidity and *E.*

coli was found. The best predictor of *E. coli* concentration was the combination of the regression-based clogging rate and turbidity (Table 5). However, contrary to expectations based on the strong linear correlation ($R^2=0.93$) between the regression-based rate of clogging and the rate calculated from the starting and ending times (endpoint method), the latter was less able to predict the concentration of *E. coli* even when combined with turbidity. The strongest relationship using the clogging rate determined by endpoints as one regressor made use of turbidity as a second regressor to predict the number of total coliforms ($R^2 = 0.93$).

According to the summary of regression analyses presented in Table 5, section 4.6, turbidity is a much less significant factor than the clogging rate. However there is a clear pattern—when turbidity is used in conjunction with clogging rate to predict general coliform concentration, the coefficient for turbidity is positive; whereas, when used to predict *E. coli* concentration, the coefficient is negative. The likely explanation for this is that general coliforms and turbidity are more strongly correlated than *E. coli* and turbidity. When modeling *E. coli* concentrations alone, the coefficient for turbidity is negative because it is subtracting off the portion of clogging that is explained by turbidity and general coliforms.

Another noteworthy aspect of the models presented in Table 5 of section 4.6 is the variety of intercepts and their associated standard error turbidity. The model intercepts range from -39.3 to -16.3 CFUs/100mL for *E. coli* and 3.46 and 12.61 CFUs/100mL for total coliforms. The negative intercepts convey that, in the prediction of *E. coli* concentration, the clogging rate will typically be greater than zero even if the turbidity and *E. coli* concentration are both zero. The intercepts for the clogging rate axis, when the turbidity and *E. coli* concentration are both zero, range from 0.08 to 0.11 mL/s/cm² per mL filtered. The positive intercepts for the total coliforms indicate that the probable number of total coliforms is greater than zero even when the clogging rate appears to be zero. This may be due to the fact that even very clean water can contain general coliforms since they are so common; however more sample needs to be filtered to build up a significant amount of foulant. Alternatively, a non-linear model may be more appropriate for very clean samples. The detection limit can be calculated in this instance as the positive intercept plus three times the standard error of the intercept. The lowest detection limit explaining total coliforms was found to be 69 CFUs/100mL using clogging rate as the sole regressor. The lowest detection limit for *E. coli* is 41 CFUs/100mL; this detection limit lies in the WHO high risk category of drinking water. This means that, with the current data set and analysis method, this assay can only discern effluent quality that carries a high or very high risk of pathogenic activity.

There were a limited number of samples that represented the high clogging rate, high bacterial concentration and very low clogging rate and very low bacterial concentration groups. The main concern is that only 6 out of 19 samples were recorded in the 100-800 CFUs/100mL total coliform and clogging rate >0.5 group (Table 7). These likely acts as leveraging points and skew the slope of the regression line used to describe total coliform concentration using the clogging rate and turbidity. In order to improve the validity of these results, more samples need to be analyzed.

The breakthrough of some turbidity into the biosand filter effluent and the occasional significance of turbidity in explaining bacterial concentrations indicate that turbidity should be measured to guarantee that it is not a confounding variable.

The replicate measurements performed for the samples collected from filter 1 on 2/4/15 and 2/12/15 resulted in respective relative standard deviations of 3% and 6%. These are negligible compared to the

uncertainty in each slope when determined via linear regression. The real limiting factor on the accuracy of the filter clogging result is the determination of the rate via the endpoint method. As a result, replicate assays were not performed for any other samples.

5.5 Limitations of the filter clogging assay

This method is only valid for Fisher Brand, 33 mm diameter, 0.2µm nylon syringe filters. A major limitation is the fact that the filters represent a disposable supply that must be replenished. It is expected that changes in manufacturing, materials, or construction can produce widely variable results. As shown, in Table 6, the baseline membrane resistance of membranes depends largely on the effective pore size and the filter material. The nylon-6,6 membrane material for 0.45µm filter has a greater resistance than any other material. However, the pore size has the greater effect on the membrane resistance. As calculated from Darcy's Law the average clean water resistance of the 0.2µm filters used in this experiment was measured to be $1.48\text{E}+11 \pm 4.29\text{E}+09 \text{ m}^{-1}$, which is over five times that of the 0.45µm nylon filter listed in Table 6. The difference is clearly due to the difference in pore size. The 0.2µm nylon filter was selected for this study in order to ensure that all bacteria were being captured and reduce the volume of sample required and the analysis time by encouraging faster clogging. However, since 0.45µm filters should be sufficient to trap almost all bacteria, especially those that are pathogenic indicators, and given that filter with larger pore size are cheaper, it would be worthwhile to perform this experiment again using 0.45µm filters to determine whether an equally useable relationship between the clogging rate and indicator bacteria is obtained.

Table 6: Membrane resistances for 0.45µm filter membranes from A. Alhadidi et al. 2011

| Material | $R_m [\times 10^{10} \text{ m}^{-1}]$ |
|-------------------|---------------------------------------|
| Nylon-6,6 | 2.65 |
| Cellulose acetate | 0.85 |
| PVDF | 0.83 |
| Cellulose acetate | 0.74 |
| Acrylic polymer | 0.66 |
| Nitro cellulose | 0.64 |
| PTFE | 0.41 |
| Polycarbonate | 0.39 |

While the consistency of individual filters in determining the clogging factor was verified to some degree, the consistency of the clogging rate for individual syringes was not investigated; this was partially due to qualitative assessments of the syringe construction and plunger resistance. It was assumed that any differences impacting the flux would be insignificant compared to the changes in flux due to clogging or difference due to filter construction. Still, to complete the development of this method, the independence of the assay results from the syringes used should be verified. Some variability in filter dimensions was apparent in the filter clogging assays where flux seemed to increase as after passing the 9mL mark and then again after passing the 1mL mark.

Future experiments should include a measure of actual pathogen concentrations since *E. coli* are only an indicator of pathogenicity. By quantifying concentrations of actual pathogen such as *Giardia* or *Cryptosporidium*, the rates of false positives and false negatives could be determined.

5.6 Ruggedness & Feasibility of the filter clogging assay

One aspect of the assay that must be addressed is the durability of the syringe and weight support system. The syringes are constructed from 1-2 mm thick, clear polypropylene with a rubber seal on the plunger. During the course of the experiment, two types of wear on the syringe were observed. First, there was a gradual increase in the kinetic frictional coefficient of the rubber seal that caused the initial flux to decrease from sample to sample over time (Figure 29). The slow decline in the clean water flux of each filter is a minor concern since this merely shifts the position of the clogging rate curve and only slightly affects the slope of this curve in the linear region. The increase in the kinetic coefficient of friction will reduce the pressure applied to the sample resulting in a more rapid clogging rate. Secondly, it was observed that over time the rubber cracks and abrades off—this degradation may be due to ozonolysis. If this is true, then time limits the durability of the syringe. However, there is the possibility that the degradation is due to mechanical wear, in which case the number of filtrations performed limits the life of the syringe. Regardless of the degradation mechanism, it would be prudent to change out the syringe every year or every 10 samples. When the syringes were swapped out in the course of this experiment, the clean water flux increased to range observed at the start of the experiment. There was no significant difference observed in the clean water flux through the filters for the first 5 assays—the syringes appear to have relatively similar frictional forces opposing the weight and have relatively little influence on the flux.

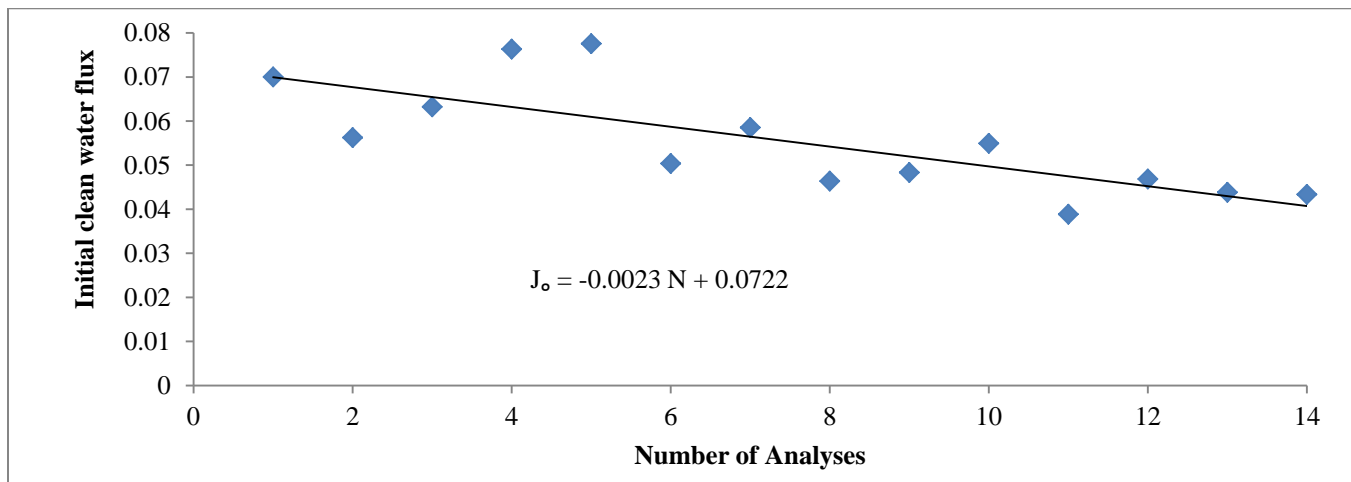


Figure 29: The initial clean water flux for each micropore filter determined using DI water prior to running each sample. The negative slope is interpreted as being caused by degradation of the syringe. After 14 samples, the syringe plunger fractured and the entire syringe was replaced.

In addition to the wear on the rubber, the simple design for hanging the mass on the plunger tended to cause the user to apply sufficient stress to the plunger to cause fatigue fractures that rendered it useless. The prototype presented in section 5.8 will avoid these stresses by employing a more stable weight hanger system. Another major issue is that the 1mL graduations on the side of the syringe are not very durable and will become illegible rapidly if not protected. This can be avoided by applying a piece of tape over the outside of the syringe. Some syringe models have graduated markings molded into the plastic, so they can't rub off, though this might represent an additional expense.

By using the filter clogging rates to model the WHO risk categories introduced earlier the feasibility of this assay was increased greatly by simplifying the interpretation of the results. The clogging rate ranges

corresponding to each risk category were determined using a power fit to the average clogging rate versus the risk category (with integers 1-4 corresponding to the respective risk categories). The power fit was evaluated at 1.5, 2.5, and 3.5 to yield the bin ranges presented in the first column of Table 7. It is expected that these categories will be further refined as the sample size is increased. Most importantly, the low risk (n=2) and high risk (n=5) categories need substantially more data points. Furthermore, this method does not take into account the effect of turbidity. A turbidity-based adjustment to the clogging rate value might be effective at improving the accuracy of these categories.

Table 7: Clogging rate ranges corresponding to a WHO drinking water risk category and the sample size on which each category is based.

| Clogging rate (mL/s/cm ² per mL filtered) | Risk category | <i>E. coli</i> range (CFUs/100mL) | Sample size |
|--|---------------|-----------------------------------|-------------|
| < 0.06 | Low | < 1 | 2 |
| 0.06 - 0.20 | Intermediate | 1 - 10 | 5 |
| 0.20 - 0.50 | High | 10 - 100 | 8 |
| > 0.50 | Very High | > 100 | 6 |

5.7 Cost and efficiency of the filter clogging assay (FCA)

On average, the cost of each FCA analysis would be around \$1.50 (Appendix 9.5, Table 9) if a single filter is consumed. This is approximately half of the cost of a bacterial assay such as Coliscan membrane filtration which is estimated to cost around \$2.80 per sample. The required supplies for the filter clogging assay are very easy to come by and have a very long storage life whereas the Coliscan MF growth medium has a limited shelf life (1 year) and must be kept frozen until use and refrigerated after opening.

The average time required to perform the FCA was 14.5±2.1 minutes. The analysis duration is dependent on the quality of the sample, resulting in a range of 10 to 23 minutes. Microbial assays typically require approximately 10 minutes of sample processing, 24 hours of incubation, and 1-10 minutes of analysis. Using 60mL syringes, which are sturdier and commonly available, would allow the assay to be performed in around 8 minutes on average. The volunteer performing the assay would allow the first 20 mL to pass through, start the timer at 40mL, stop it at 30mL, let the remainder pass through, and finally then take up another and other 60mL and repeat the same process. The results obtained by this method would be more accurate. Though the flow rate would be the same if the weight applied was increased, the plunger would be moving slower making it easier to record the times accurately. Since removing the filter and refilling the syringe, can introduce additional random and systematic error, avoiding as much as possible this would improve the accuracy of the assay.

5.8 The prototype assay kit and protocol

With the clogging rates categorized into the 4 WHO risk factors according to their respective *E. coli* concentrations, the detection limit was calculated to include only half of the medium risk category. Also the average clogging rate for each category proved to be significantly different at the 90% significance level. The significance level is expected to increase as more samples are taken.

In order to be certain that the proposed assay is simple and robust enough to be useful in the field and understandable by those without personal instruction volunteers should be asked to perform the assay using the kit illustrated in Figure30 and the instructions presented below in Figure 31.

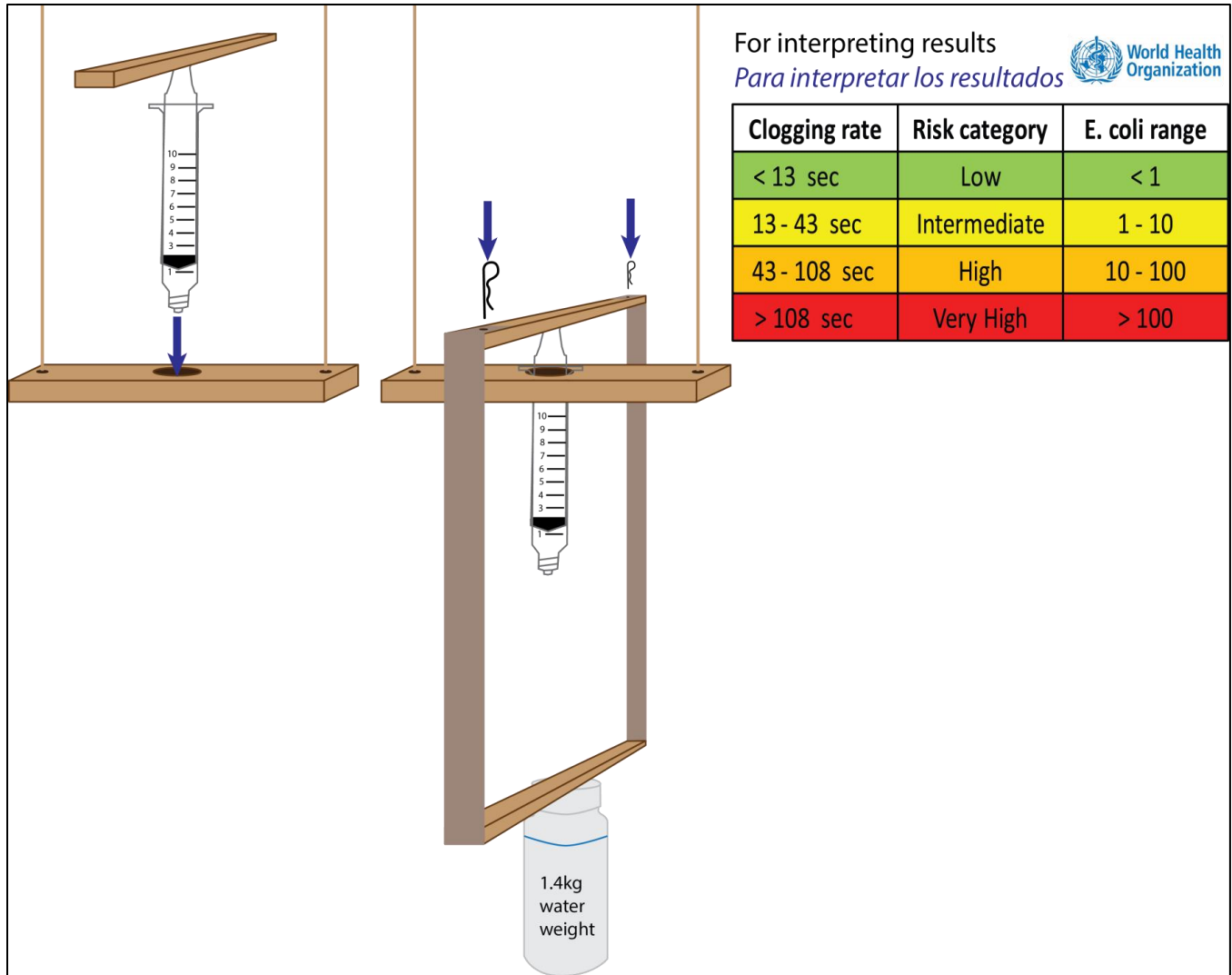


Figure 30: Instructions for assembling the assay kit and including the assay interpretation.

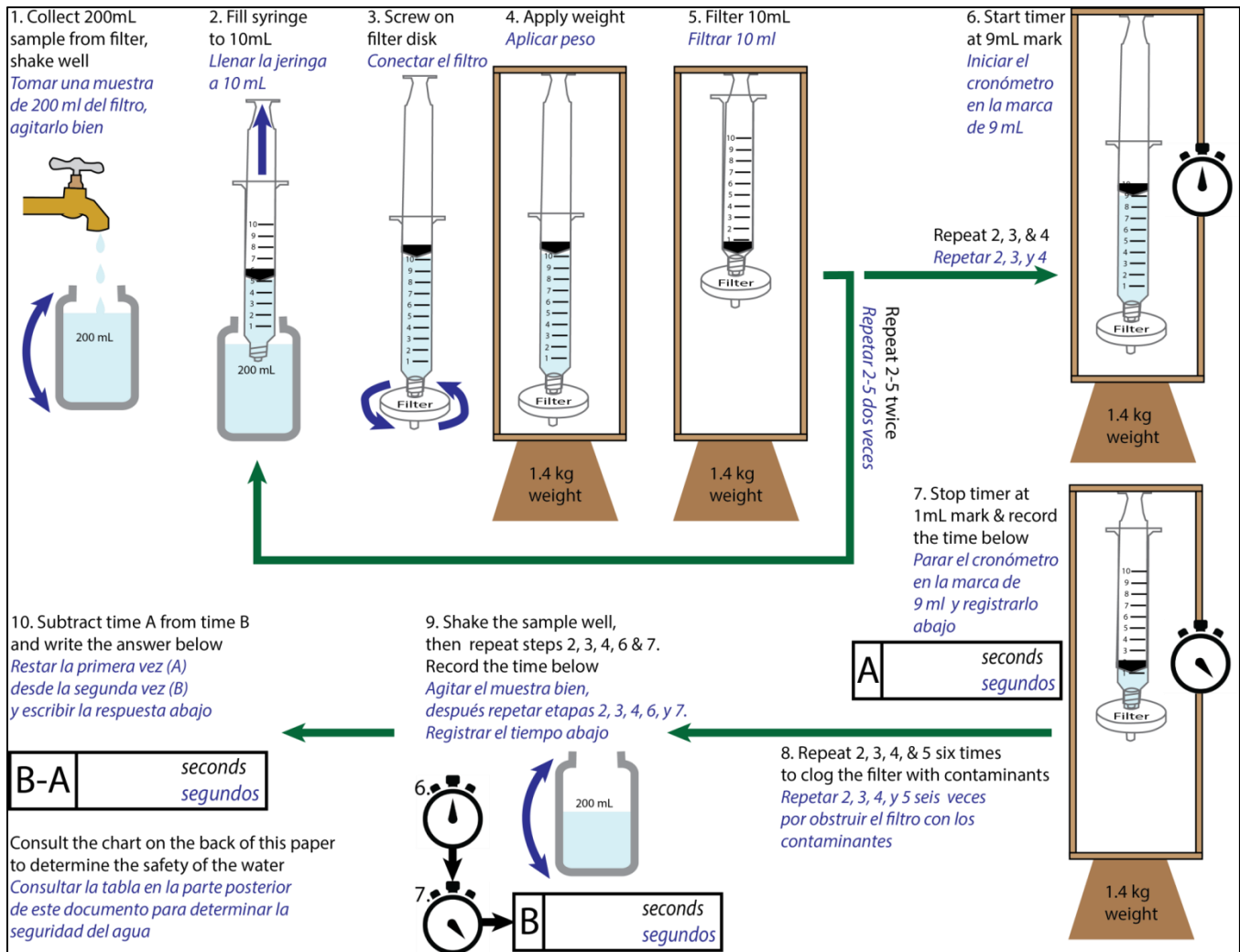


Figure 31: Instructions for performing the assay.

6 Conclusions

Ultimately, the filter clogging assay described here is effective at determining the probable WHO risk category of a filter effluent in less than 15 minutes at an average cost of \$1.50 per sample. This method would greatly enhance the decision-making process for water system managers and health workers, resulting in fewer illnesses and outbreaks. The filter clogging rate determined by regression alone was more effective at predicting the number of total coliforms ($R^2 = 0.93$, $p = 6.5E-10$) than turbidity ($R^2 = 0.74$, $p = 9.6E-06$). For clogging rates determined by the endpoint method, turbidity and the clogging rate combined were more effective than any other single factor at predicting the number of total coliforms ($R^2 = 0.93$, $p = 3.6E-08$).

Initial attempts to identify a simple infrared (IR) colorimetry or capacitance measurement technique for assessing either biolayer maturity or effluent quality led to the conclusion that such methods would be relatively ineffective (IR) or too costly or complicated (capacitance measurement) to justify their use in the field in preference to other cheaper (turbidity) or more effective (bacterial cultures) tools.

The bacterial assays performed for the FCA experiment indicate that biosand filter effluent is seldom, if ever, sterile—general coliforms and *E. coli* are still found in varying concentrations in the outflow. This is expected, there is a reason for the common practice in developed nations of following a sand filtration stage with a UV or chemical disinfection stage. The biosand filter is most effective at polishing a water source before final treatment. It is recommended that when possible, a UV lamp, or other disinfecting solution, be installed on the outlet.

This work has also furthered the understanding of the breakthrough of turbidity in biosand filters. The positive correlation between influent and effluent turbidity indicates that the ability of a biosand filter to remove turbidity is variable and there can be significant breakthrough of smaller particles, especially when water with high a concentration of suspended clay is used as the influent. Contrary to initial expectations, effluent turbidity is high enough under some conditions to include it as a regressor in the model for total coliforms. This is supported by a comparison of the model clogging rate model with and model without turbidity as a regressor.

Improvements to the FCA assay may be realized with the use of a filter with a 0.45 μ m pore size or the use of a larger 60mL syringe. Also correlations with actual pathogen counts and a greater number of samples are essential to establishing the accuracy and significance of this assay.

Finally, it is proposed that the first implementations of this assay be in estimations of the WHO risk category of drinking water in developing nations. To work towards this goal, volunteer focus groups must be organized to gather data and evaluate the assay equipment and method using actual biosand effluent. As soon as the method is finalized, a much larger calibration data set with hundreds of data points must be generated by a wide range of researchers using the same bacterial and filter clogging assay methods. It is very likely that the filter clogging assay can be applied to effluent from numerous other treatment systems and may be appropriate for testing low turbidity surface water.

7 Acknowledgments

My sincere thanks to Dr. Jon Erickson, my advisor, for his guidance and help puzzling through the many experiments in this work. Thank you also to Department of Physics and Engineering for the lab space and funding, Dr. Paul Low (Geology) for help with various analyses, Emily Flowers (Geology) and Dave Pfaff for help with the SEM, Dr. Bill Hamilton (Biology) for lab space, equipment, and supplies needed to perform the bacterial assays, W&L Engineers Without Borders for the inspiration to carry out this project, the Department of Chemistry and Biochemistry for use of the IR spectrometer, Haley Smith for helping me edit my Spanish translation for the FCA manual, and Chad & Lisa Hammond for copy editing this work.

8 References

- [1] Aiken, B. A., Stauber, C. E., Ortiz, G. M. & Sobsey, M. D. An Assessment of Continued Use and Health Impact of the Concrete Biosand Filter in Bonao, Dominican Republic. *Am J Trop Med Hyg* 85, 309–317 (2011). Alhadidi, A. et al. Silt Density Index and Modified Fouling Index relation, and effect of pressure, temperature and membrane resistance. *Desalination* 273, 48–56 (2011).
- [2] Angaji, M. T., Zinali, A. Z. & Qazvini, N. T. Study of Physical, Chemical and Morphological Alterations of Smectite Clay upon Activation and Functionalization via the Acid Treatment. *World Journal of Nano Science and Engineering* 03, 161–168 (2013).

- [3] ASTM International. Standard Test Method for Silt Density Index (SDI) of Water. (ASTM International, 2002).
- [4] Baker, R. W. Membrane Technology and Applications. (Wiley, 2012).
- [5] Berg, M. et al. Arsenic Contamination of Groundwater and Drinking Water in Vietnam: A Human Health Threat. *Environ. Sci. Technol.* 35, 2621–2626 (2001).
- [6] Bowen, W. R., Calvo, J. I. & Hernández, A. Steps of membrane blocking in flux decline during protein microfiltration. *Journal of Membrane Science* 101, 153–165 (1995).
- [7] Bradley, I., Straub, A., Maraccini, P., Markazi, S. & Nguyen, T. H. Iron oxide amended biosand filters for virus removal. *Water Research* 45, 4501–4510 (2011).
- [8] Brookes, J. D. et al. Relative Value of Surrogate Indicators for Detecting Pathogens in Lakes and Reservoirs. *Environ. Sci. Technol.* 39, 8614–8621 (2005).
- [9] Davis, R., Irudayaraj, J., Reuhs, B. L. & Mauer, L. J. Detection of *E. coli* O157:H7 from Ground Beef Using Fourier Transform Infrared (FT-IR) Spectroscopy and Chemometrics. *Journal of Food Science* 75, M340–M346 (2010).
- [10] Divelbiss, D. W., Boccelli, D. L., Succop, P. A. & Oerther, D. B. Environmental Health and Household Demographics Impacting Biosand Filter Maintenance and Diarrhea in Guatemala: An Application of Structural Equation Modeling. *Environ. Sci. Technol.* 47, 1638–1645 (2013).
- [11] Djongoue, P. & Njopwouo, D. FT-IR Spectroscopy Applied for Surface Clays Characterization. *Journal of Surface Engineered Materials and Advanced Technology* 03, 275–282 (2013).
- [12] Elliott, M. A., Stauber, C. E., Koksal, F., DiGiano, F. A. & Sobsey, M. D. Reductions of *E. coli*, echovirus type 12 and bacteriophages in an intermittently operated household-scale slow sand filter. *Water Research* 42, 2662–2670 (2008).
- [13] Edberg, S. c., Rice, E. w., Karlin, R. j. & Allen, M. j. *Escherichia coli*: the best biological drinking water indicator for public health protection. *Journal of Applied Microbiology* 88, 106S–116S (2000).
- [14] Field, R. W., Wu, D., Howell, J. A. & Gupta, B. B. Critical flux concept for microfiltration fouling. *Journal of Membrane Science* 100, 259–272 (1995).
- [15] Holdich, R., Kosvintsev, S., Cumming, I. & Zhdanov, S. Pore design and engineering for filters and membranes. *Philosophical Transactions of the Royal Society of London A: Mathematical, Physical and Engineering Sciences* 364, 161–174 (2006).
- [16] Howe, K. J., Ishida, K. P. & Clark, M. M. Use of ATR/FTIR spectrometry to study fouling of microfiltration membranes by natural waters. *Desalination* 147, 251–255 (2002).
- [17] Huisman, L. & Wood, W. E. in (The World Health Organization, 1974).
- [18] Katti, K. S. & Katti, D. R. Relationship of Swelling and Swelling Pressure on Silica–Water Interactions in Montmorillonite. *Langmuir* 22, 532–537 (2006).
- [19] Konieczny, K. Modelling of membrane filtration of natural water for potable purposes. *Desalination* 143, 123–139 (2002).
- [20] Kremen, S. S. & Tanner, M. Silt density indices (SDI), percent plugging factor (%PF): their relation to actual foulant deposition. *Desalination* 119, 259–262 (1998).
- [21] Kroukamp, O. & Wolfaardt, G. M. CO₂ Production as an Indicator of Biofilm Metabolism. *Appl. Environ. Microbiol.* 75, 4391–4397 (2009).
- [22] Lim, A. L. & Bai, R. Membrane fouling and cleaning in microfiltration of activated sludge wastewater. *Journal of Membrane Science* 216, 279–290 (2003).
- [23] Liu, Y.-J. & Sun, D. D. Particles size-associated membrane fouling in microfiltration of denitrifying granules supernatant. *Chemical Engineering Journal* 181–182, 494–500 (2012).

- [24] Lloyd, B. J. & Bartram, J. K. Surveillance Solutions to Microbiological Problems in Water Quality Control in Developing Countries. *Wat. Sci. Tech.* 24, 61–75 (1991).
- [25] Métris, A., George, S. M., Peck, M. W. & Baranyi, J. Distribution of turbidity detection times produced by single cell-generated bacterial populations. *Journal of Microbiological Methods* 55, 821–827 (2003).
- [26] Miller, K. Defluoridation of Drinking Water Using Appropriate Sorption Technologies. *Proceedings of the Water Environment Federation* 2007, 9245–9254 (2007).
- [27] Myre, E. & Shaw, R. *The Turbidity Tube: Simple and Accurate Measurement of Turbidity in the Field.* (2006).
- [28] Nakada, N. et al. Removal of selected pharmaceuticals and personal care products (PPCPs) and endocrine-disrupting chemicals (EDCs) during sand filtration and ozonation at a municipal sewage treatment plant. *Water Research* 41, 4373–4382 (2007).
- [29] Ngai, T. K. K., Murcott, S., Shrestha, R. R., Dangol, B. & Maharjan, M. Development and dissemination of Kanchan™ Arsenic Filter in rural Nepal. *Water Science & Technology: Water Supply* 6, 137 (2006).
- [30] Noubactep, C., Temgoua, E. & Rahman, M. A. Designing Iron-Amended Biosand Filters for Decentralized Safe Drinking Water Provision. *Clean Soil Air Water* 40, 798–807 (2012).
- [31] O’Day, P., Vlassopoulos, D., Root, R. & Rivera, N. The influence of sulfur and iron on dissolved arsenic concentrations in the shallow subsurface under changing redox conditions. *PNAS* 101, 13703–13708 (2004).
- [32] Palmateer, G. et al. Toxicant and parasite challenge of Manz intermittent slow sand filter. *Environ. Toxicol.* 14, 217–225 (1999).
- [33] Pronk, M., Goldscheider, N. & Zopfi, J. Dynamics and interaction of organic carbon, turbidity and bacteria in a karst aquifer system. *Hydrogeol J* 14, 473–484 (2005).
- [34] Radke, S. M. & Alocilja, E. C. A high density microelectrode array biosensor for detection of *E. coli* O157:H7. *Biosensors and Bioelectronics* 20, 1662–1667 (2005).
- [35] Sanz, D. A., Unigarro, E. A., Osma, J. F. & Segura-Quijano, F. Low cost wireless passive microsensors for the detection of hazardous compounds in water systems for control and monitoring. *Sensors and Actuators B: Chemical* 178, 26–33 (2013).
- [36] Schmitt, J. & Flemming, H.-C. FTIR-spectroscopy in microbial and material analysis. *International Biodeterioration & Biodegradation* 41, 1–11 (1998).
- [37] Schwartz, J., Levin, R. & Hodge, K. Drinking water turbidity and pediatric hospital use for gastrointestinal illness in Philadelphia. *Epidemiology* 8, 615–620 (1997).
- [38] Stauber, C. E. et al. Characterisation of the biosand filter for *E. coli* reductions from household drinking water under controlled laboratory and field use conditions. *Water Sci. Technol.* 54, 1–7 (2006).
- [39] Stauber, C. E., Printy, E. R., McCarty, F. A., Liang, K. R. & Sobsey, M. D. Cluster Randomized Controlled Trial of the Plastic BioSand Water Filter in Cambodia. *Environ. Sci. Technol.* 46, 722–728 (2012).
- [40] Tiwari, S. S. K.; Schmidt, W. P.; Darby, J.; Kariuki, Z. G.; Jenkins, M. W. Intermittent slow sand filtration for preventing diarrhea among children in Kenyan households using unimproved water sources: Randomized controlled trial. *Trop. Med. Int. Health*, 14, 1374–1382 (2009)
- [41] Vrana, B. et al. Passive sampling techniques for monitoring pollutants in water. *TrAC Trends in Analytical Chemistry* 24, 845–868 (2005).
- [42] WHO. *Guidelines for Drinking-water Quality* (4th edition. (2011).
- [43] WHO. *Progress on drinking water and sanitation.* (2014).

- [44] Yang, L., Li, Y. & Erf, G. F. Interdigitated Array Microelectrode-Based Electrochemical Impedance Immunosensor for Detection of *Escherichia coli* O157:H7. *Anal. Chem.* 76, 1107–1113 (2004).
- [45] Young-Rojanschi, C. & Madramootoo, C. Intermittent versus continuous operation of biosand filters. *Water Research* 49, 1–10 (2014).
- [46] Young-Rojanschi, C. & Madramootoo, C. Comparing the performance of biosand filters operated with multiday residence periods. *Journal of Water Supply: Research and Technology—AQUA* 64, 157 (2015).

9 Appendices

9.1 Calibration data

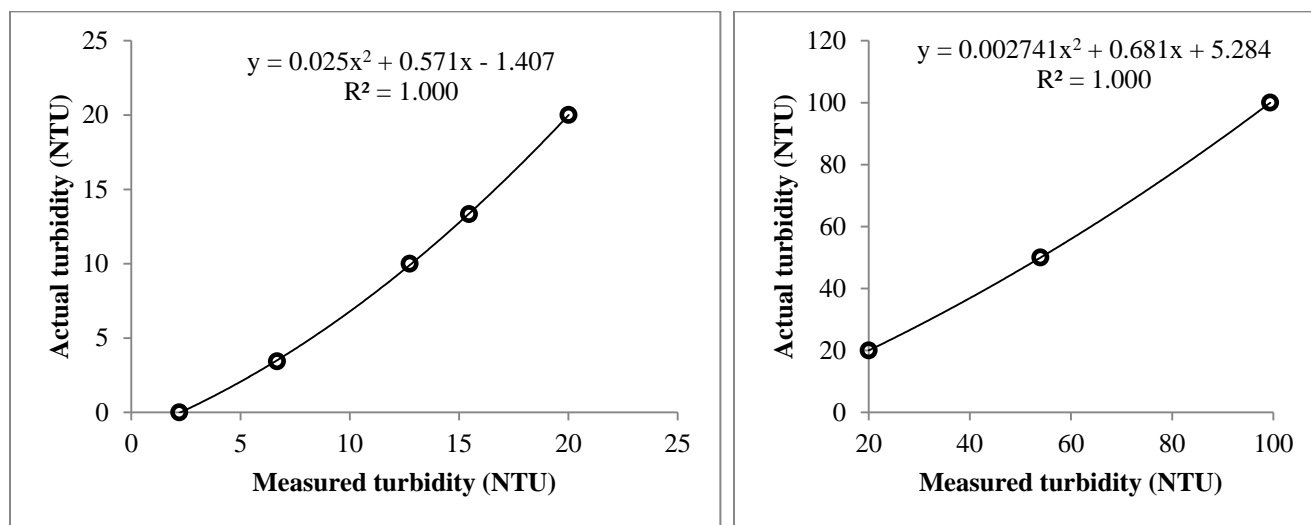


Figure 32: (left) A polynomial calibration curve for low-range (0-20 NTUs) turbidity measurements using a Neulog turbidity meter to measure a 20 NTU standard, three dilutions of that standard, and a filtered DI water blank. (right) A calibration curve for high-range turbidity measurements (20-100 NTUs) generated from 20, 50, and 100 NTUs standards. In both cases, a high purity alcohol blank was used to subtract the light-scattering effect of any imperfections in the plastic cuvette.

9.2 FT-IR of filters

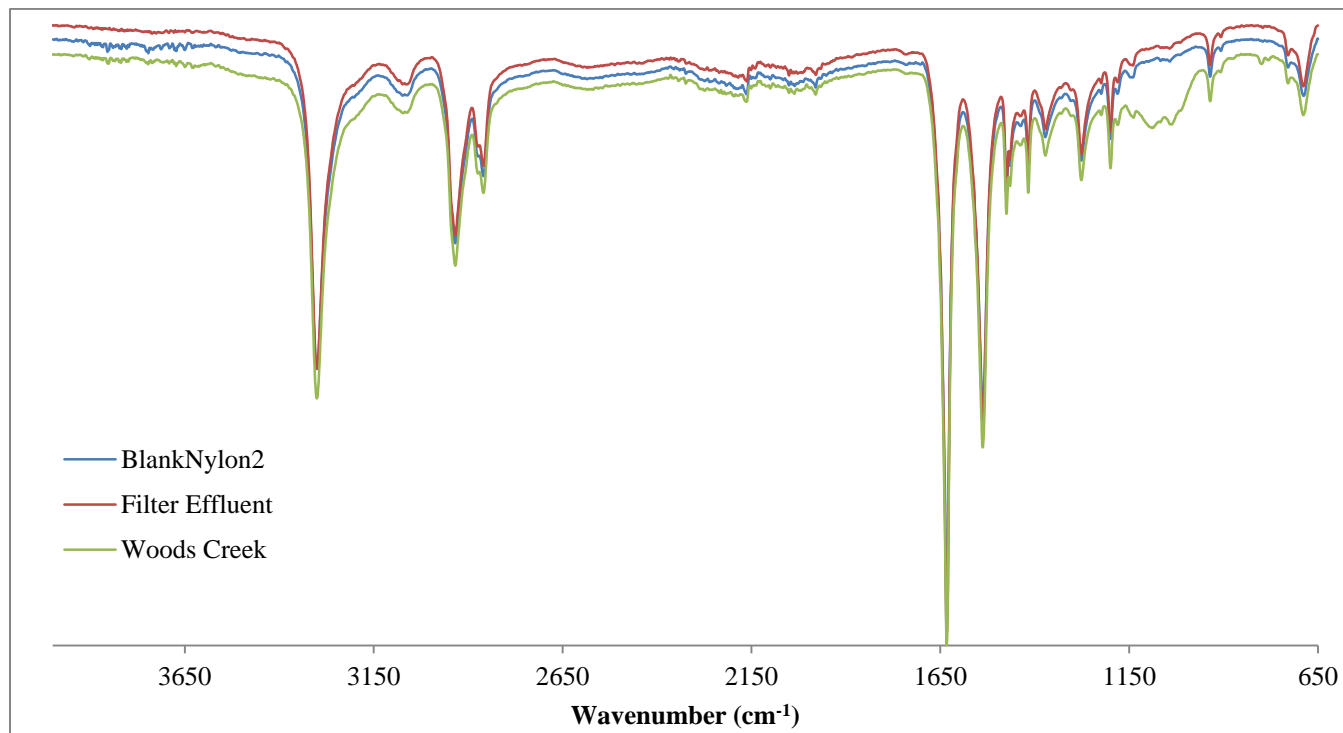


Figure 33: IR spectra of a nylon filter (Filter Effluent) used for sample from filter 1 on January 20th (Turbidity = 0.08 NTUs) and nylon filter3 used to analyze sample from Woods Creek on March 7th (Turbidity = 2.35 NTUs) compared with a blank (unused) nylon filter.

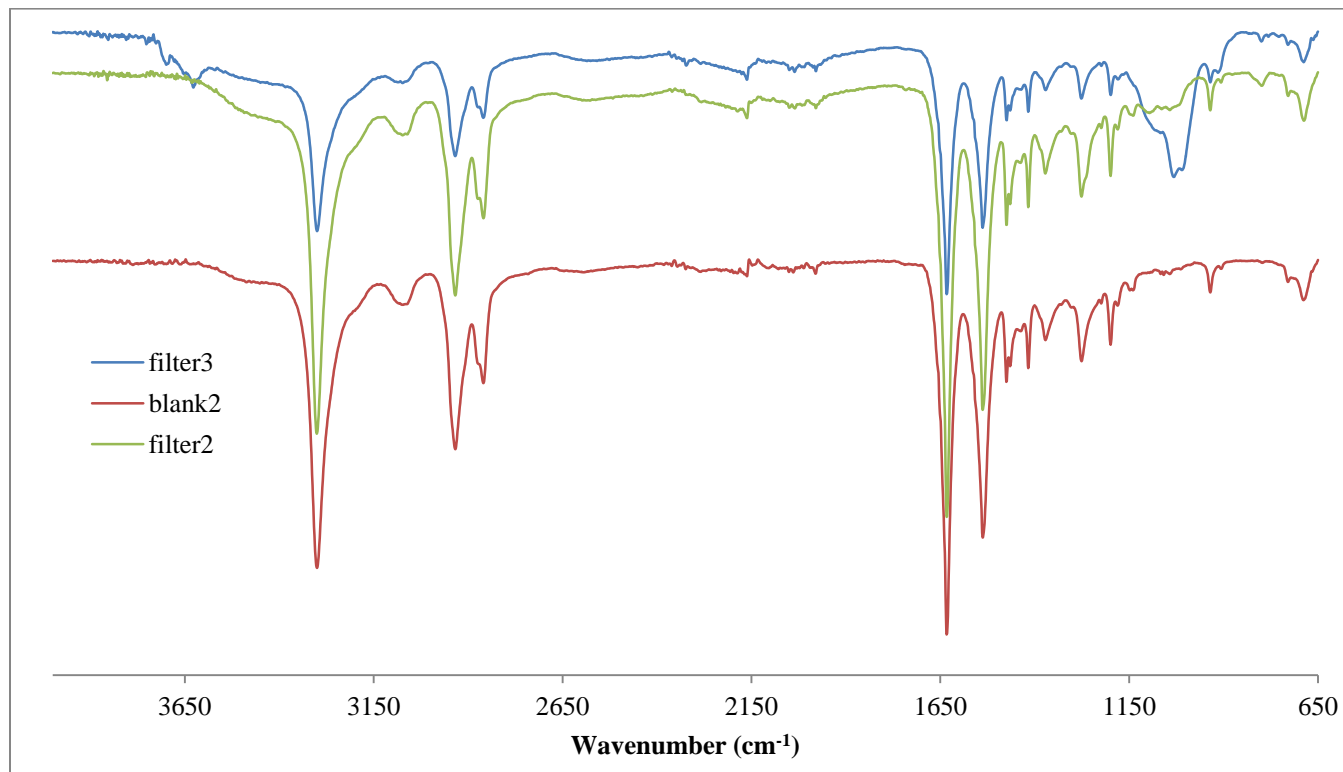
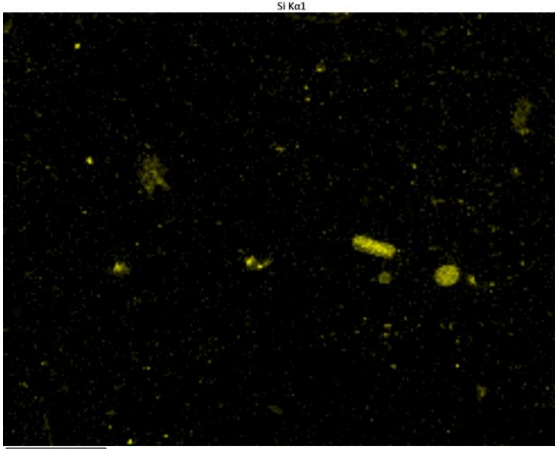
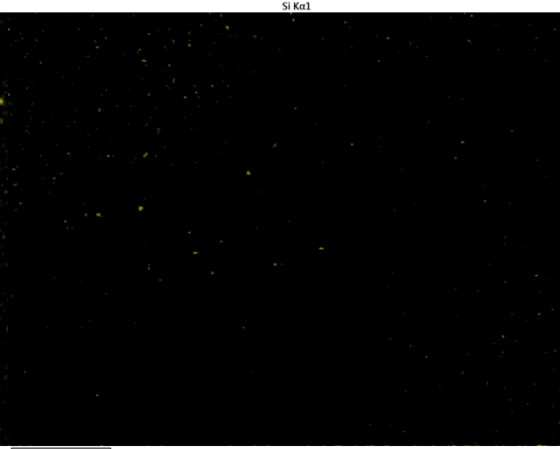
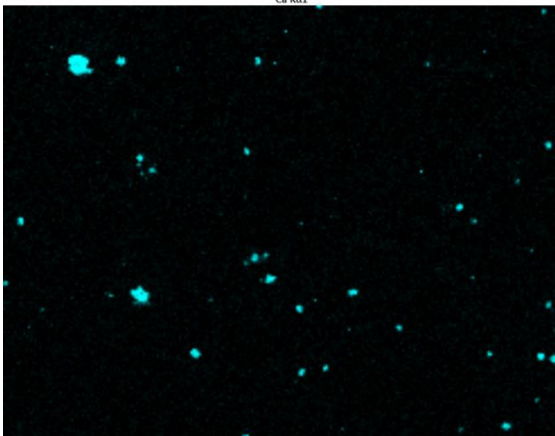
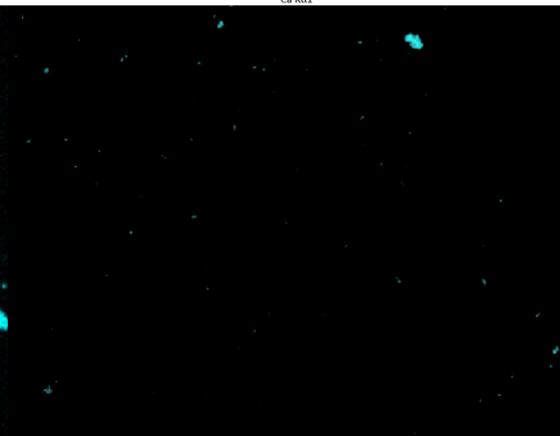
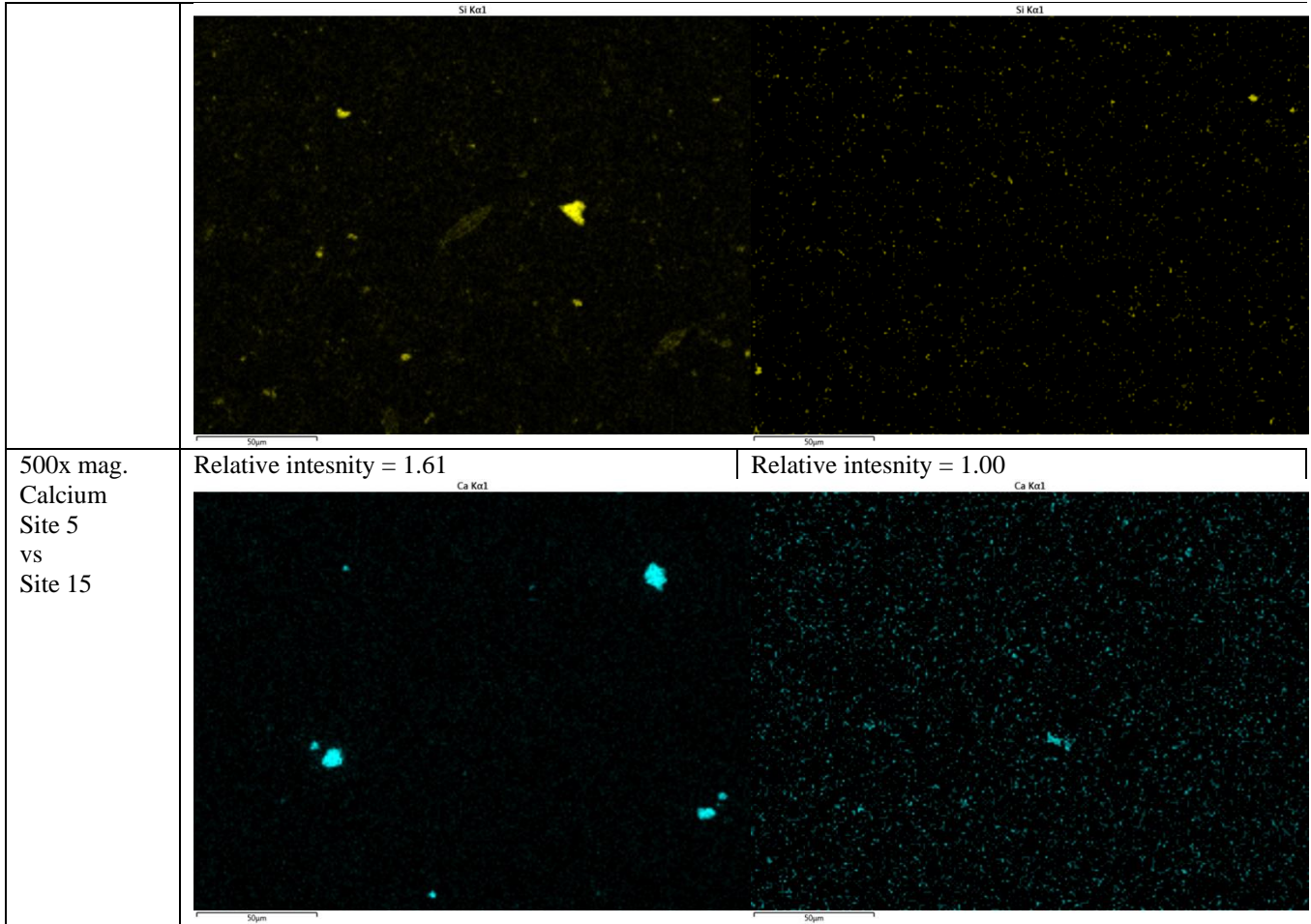


Figure 34: IR spectra of nylon filter2 used for sample from filter 1 on March 5th (Turbidity = 0.91 NTUs) and nylon filter3 used to analyze sample from filter 1 on March 7th (Turbidity = 4.22 NTUs) compared with a blank (unused) nylon filter.

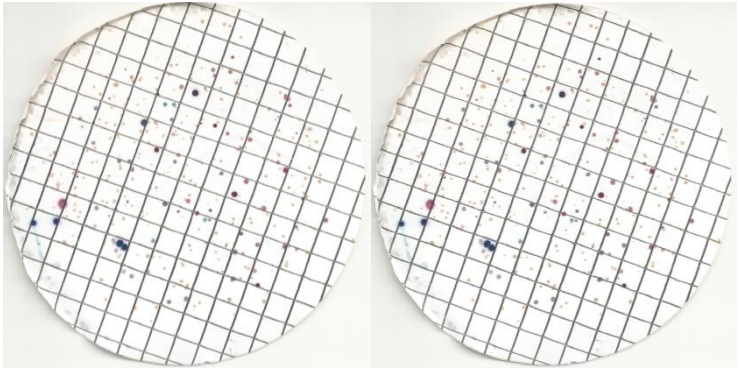
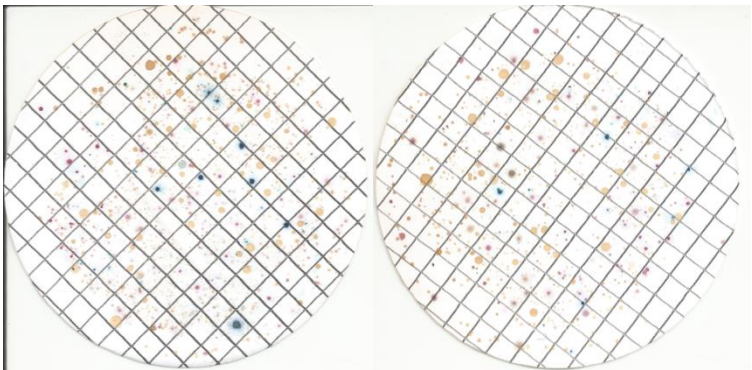
9.3 SEM-EDS micrographs

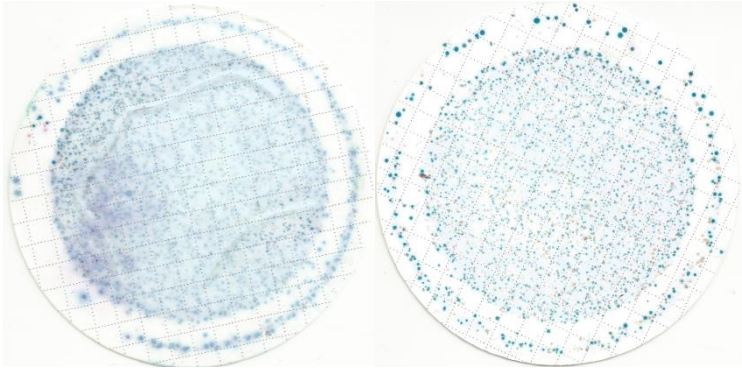
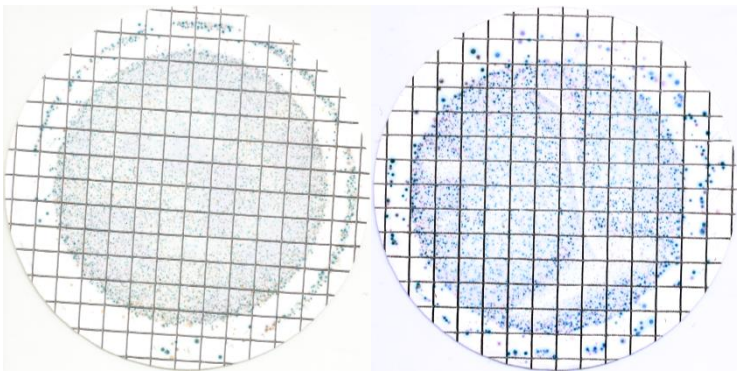
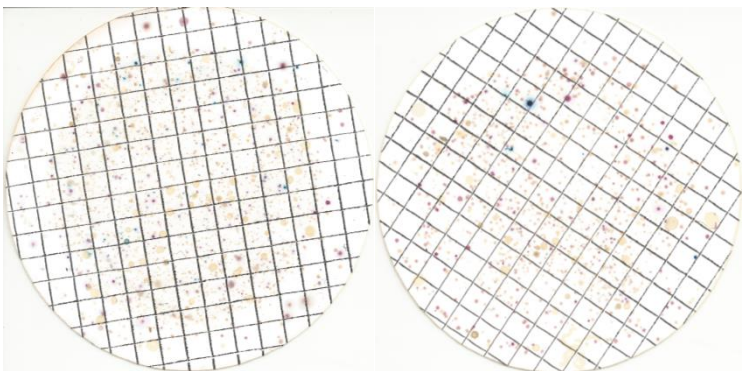
Table 8: The average intensity of the sum of the calcium and silicon signals for the filter used on biosand effluent was 31% of that of the unfiltered, low turbidity Woods Creek water. Two magnifications, 200x and 500x were used to ensure that small particles in the pores that were resolved. Relative intensities were calculated from the raw counts per second measured by the EDS and the micrographs were adjusted in intensity correspondingly since they were originally saturated.

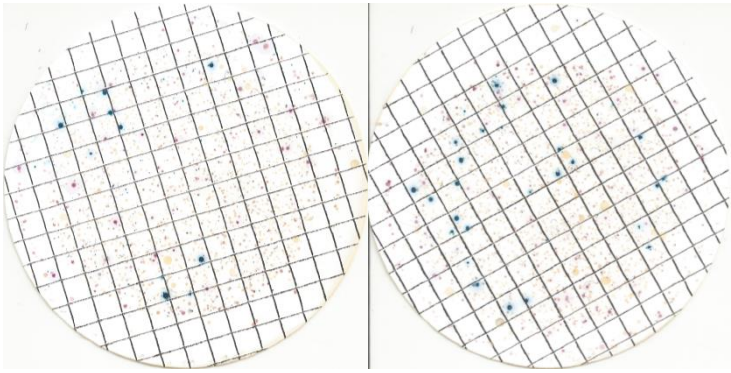
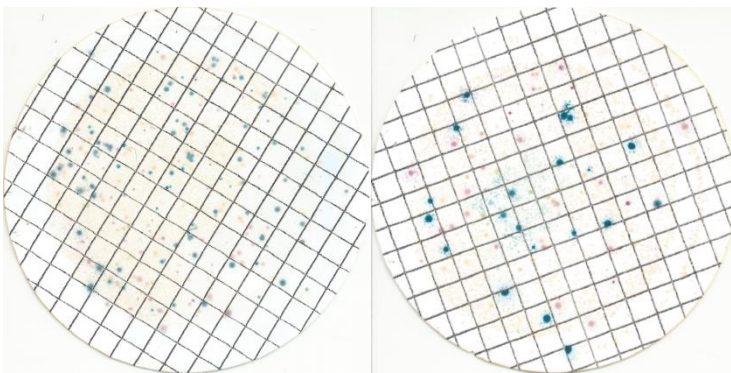
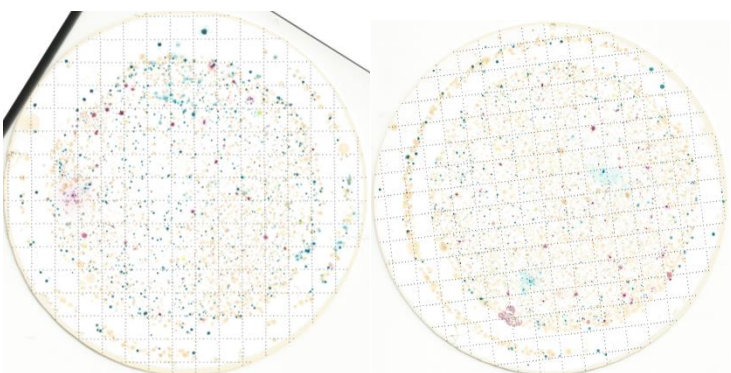
| Notes | Woods Creek unfiltered | Biosand effluent |
|---|--|---|
| 200x mag. Silicon Site 2 vs Site 12 | Relative intensity = 7.02  | Relative intensity = 1.00  |
| 200x mag. Calcium Site 2 vs Site 12 | Relative intensity = 1.68  | Relative intensity = 1.00  |
| 500x mag. Silicon Site 5 vs Site 15 | Relative intensity = 2.75 | Relative intensity = 1.00 |

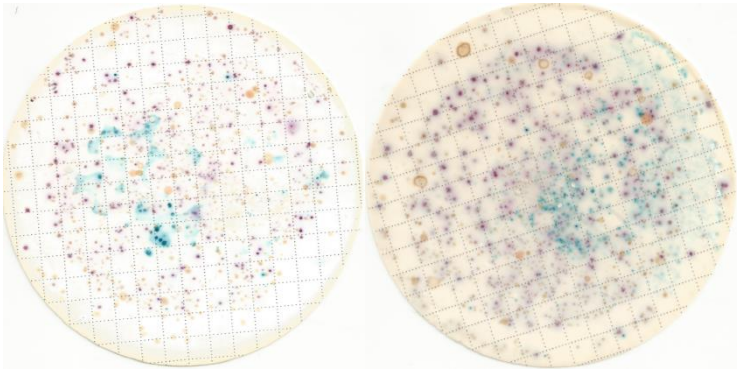
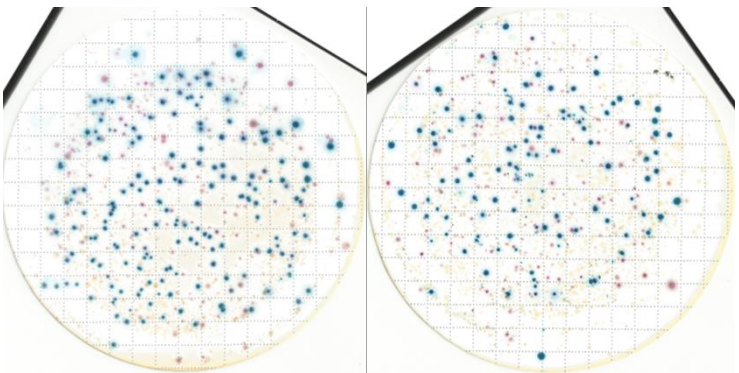
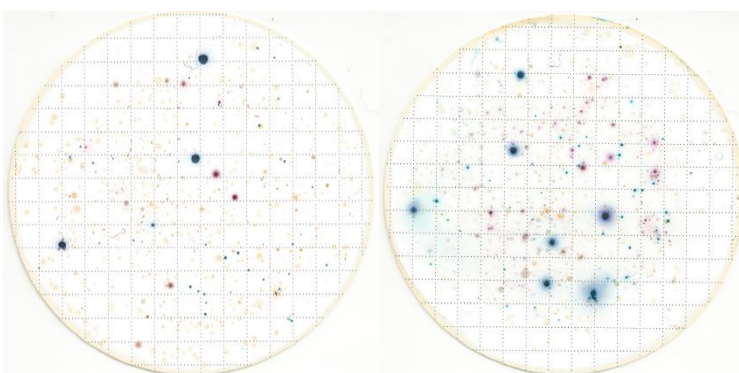


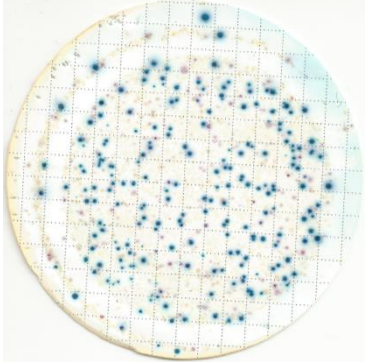
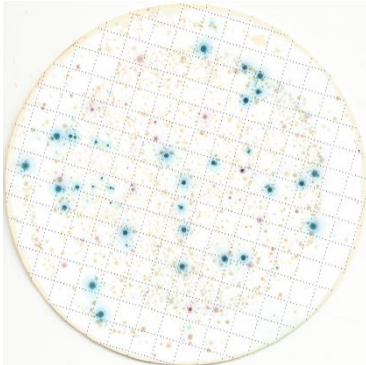
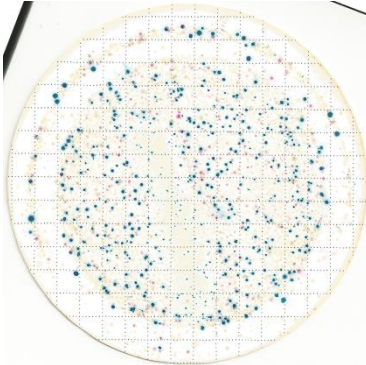
9.4 Scanned images of Coliscan bacterial cultures

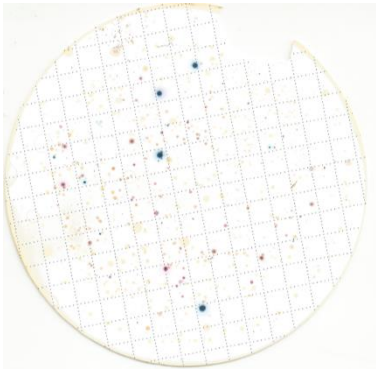
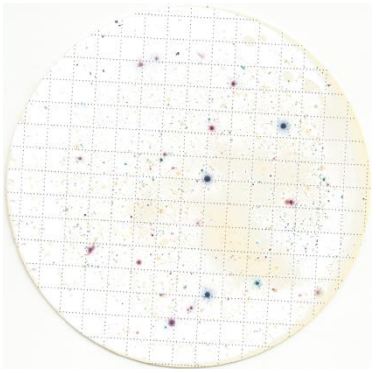
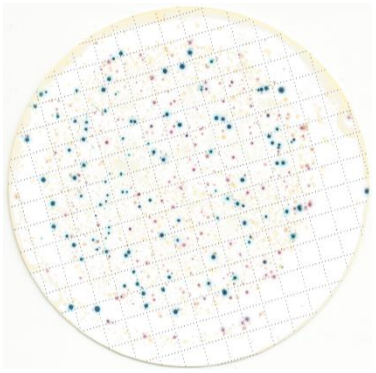
| | |
|---|--|
| <p>Sample name, date, <i>E.coli</i> and general coliform counts, turbidity, and clogging rate</p> | <p>Scanned image of bacterial plate</p> |
| <p>filter1-200mL,100mL, 1/20/15 <i>E. coli</i>: 5.3 General coliforms: 27.5 0.8 NTUs Clogging rate: 0.101 mL/s/cm² per mL filtered</p> |  |
| <p>WoodsCreek-100mL,50mL, 2/5/15 <i>E. coli</i>: 13.5 General coliforms: 70.5 2.35 NTUs Clogging rate: 0.216 mL/s/cm² per mL filtered</p> |  |

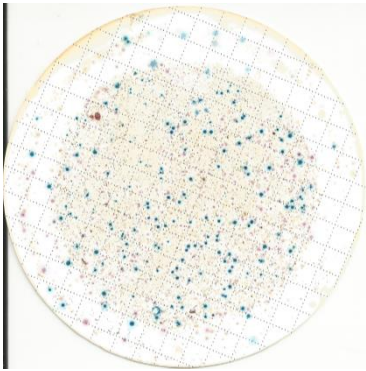
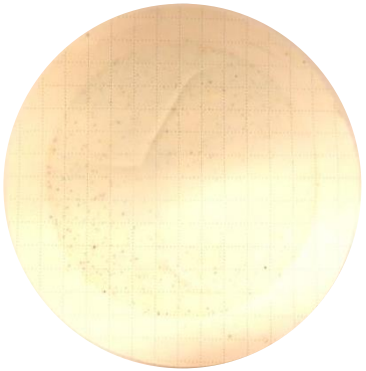
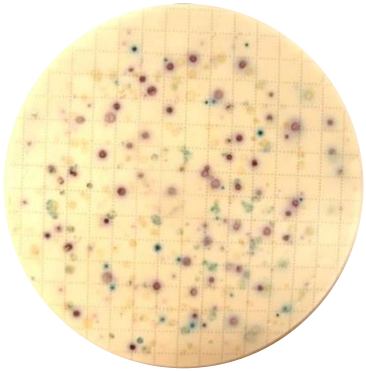
| | |
|---|--|
| <p>filter1-150mL,150mL, 2/4/15 <i>E. coli</i>: 1004.7 General coliforms: 323.5 0.11 NTUs Clogging rate: 0.362 mL/s/cm² per mL filtered</p> |  |
| <p>filter1-100mL,100mL, 2/12/15 <i>E. coli</i>: 2008.5 General coliforms: 1183.3 0.48 NTUs Clogging rate: 0.836 mL/s/cm² per mL filtered</p> |  |
| <p>filter1-200mL,100mL, 3/1/15 <i>E. coli</i>: 10.3 General coliforms: 162.0 0.6 NTUs Clogging rate: 0.295 mL/s/cm² per mL filtered</p> |  |

| | |
|---|--|
| <p>filter1-125mL,200mL, 3/5/15 <i>E. coli</i>: 17.7 General coliforms: 136.7 0.91 NTUs Clogging rate: 0.119 mL/s/cm² per mL filtered</p> |  |
| <p>filter1-50mL,200mL, 3/7/15 <i>E. coli</i>: 48.3 General coliforms: 57.8 4.22 NTUs Clogging rate: 0.571 mL/s/cm² per mL filtered</p> |  |
| <p>filter1-100mL,100mL, 3/29/15 <i>E. coli</i>: 49.0 General coliforms: 87.5 0.56 NTUs Clogging rate: 0.214 mL/s/cm² per mL filtered</p> |  |

| | |
|--|--|
| <p>filter1-120mL,200mL, 3/31/15 <i>E. coli</i>: 29.5 General coliforms: 69.5 0.85 NTUs Clogging rate: 0.202 mL/s/cm² per mL filtered</p> |  |
| <p>filter1-200mL,100mL, 4/16/15 <i>E. coli</i>: 104.5 General coliforms: 89.8 5.01 NTUs Clogging rate: 0.343 mL/s/cm² per mL filtered</p> |  |
| <p>filter1-50mL,100mL, 4/19/15 <i>E. coli</i>: 11.3 General coliforms: 65.3 3.89 NTUs Clogging rate: 0.228 mL/s/cm² per mL filtered</p> |  |

| | |
|--|--|
| <p>filter1-150mL,100mL, 4/21/15 <i>E. coli</i>: 208.0 General coliforms: 79.0 8.19 NTUs Clogging rate: 0.832 mL/s/cm² per mL filtered</p> |  |
| <p>filter1-100mL, 4/22/15 <i>E. coli</i>: 36.0 General coliforms: 58.0 5.57 NTUs Clogging rate: 0.421 mL/s/cm² per mL filtered</p> |  |
| <p>filter2-100mL, 4/22/15 <i>E. coli</i>: 429.0 General coliforms: 163.0 8.87 NTUs Clogging rate: 1.291 mL/s/cm² per mL filtered</p> |  |

| | |
|--|--|
| <p>filter1-90mL, 4/25/15 <i>E. coli</i>: 2 General coliforms: 28.4 4.18 NTUs Clogging rate: 0.033 mL/s/cm² per mL filtered</p> |  |
| <p>filter1-250mL, 4/25/15 <i>E. coli</i>: 12.2 General coliforms: 45.6 5.40 NTUs Clogging rate: 0.039 mL/s/cm² per mL filtered</p> |  |
| <p>filter2-100mL, 4/25/15 <i>E. coli</i>: 90.4 General coliforms: 107.2 5.90 NTUs Clogging rate: 0.371 mL/s/cm² per mL filtered</p> |  |

| | |
|--|--|
| <p>WC-50mL, 4/25/15 <i>E. coli</i>: 354.0 General coliforms: 472.0 24.53 NTUs Clogging rate: 1.884 mL/s/cm² per mL filtered</p> |  |
| <p>DIBlack-125mL, 4/30/15 <i>E. coli</i>: 0.0 General coliforms: 10.0 3.79 NTUs Clogging rate: 0.008 mL/s/cm² per mL filtered</p> |  |
| <p>filter1-100mL, 5/2/15 <i>E. coli</i>: 2.0 General coliforms: 32.5 4.04 NTUs Clogging rate: 0.156 mL/s/cm² per mL filtered</p> |  |

9.5 Cost comparison

Table 9: Calculations of approximate costs of the filter clogging assay and the bacteria assay per sample.

| Filter Clogging Assay items | Cost (\$) | Useful life (# samples) | Cost/sample (\$) |
|------------------------------------|------------------|--------------------------------|-------------------------|
| syringe and weight hanger | 1.00 | 1000's | 0.00 |
| weight (1.5L bottle) | 1.59 | 1000's | 0.00 |
| syringe | 0.10 | 10 | 0.01 |
| 0.2µm filter | 1.50 | 1 | 1.50 |
| TOTAL | --- | --- | 1.51 |
| Filter Clogging Assay items | Cost (\$) | Useful life (# samples) | |
| denatured alcohol (500mL) | 6.00 | 100 | 0.06 |
| tweezers | 15.00 | 1000's | 0.02 |
| refrigeration for growth medium | 165.00 | 1000's | 0.17 |
| incubator (Hovabator) | 29.99 | 1000's | 0.03 |
| vacuum apparatus | 13.52 | 1000's | 0.01 |
| Coliscan MF growth medium | 11.40 | 10 | 1.14 |
| dish with pad | 0.71 | 1 | 0.71 |
| membrane filter | 0.74 | 1 | 0.74 |
| TOTAL | --- | --- | 2.88 |